Appl. Phys. B 69, 171–202 (1999) / Digital Object Identifier (DOI) 10.1007/s003409900114

Applied Physics B
Lasers
and Optics

Invited paper

Laser intracavity absorption spectroscopy

V.M. Baev*, T. Latz, P.E. Toschek

Institut für Laser-Physik, Universität Hamburg, Jungiusstrasse 9, D-20355 Hamburg, Germany
(Fax: +49-40/42838-6571, E-mail: baev@physnet.uni-hamburg.de)

Received: 10 May 1999/Published online: 29 July 1999

Abstract. Emission spectra of multimode lasers are very sensitive to spectrally selective extinction in their cavity. This phenomenon allows the quantitative measurement of absorption. The sensitivity of measurements of intracavity absorption grows with the laser pulse duration. The ultimate sensitivity obtained with a cw laser is set by various perturbations of the light coherence, such as quantum noise, Rayleigh scattering, four-wave mixing by population pulsations, and stimulated Brillouin scattering. It depends on the particular laser type used, and on its operative parameters, for example pump power, cavity loss, cavity length, and length of the gain medium. Nonlinear mode-coupling dominates the dynamics of lasers that feature a thin gain medium, such as dye lasers, whereas Rayleigh scattering is more important in lasers with a long gain medium, such as doped fibre lasers, or the Ti:sapphire laser. The highest sensitivity so far has been obtained with a cw dye laser. It corresponds to 70 000 km effective length of the absorption path. The ultimate spectral resolution is determined by the spectral width of mode emission, which is 0.7 Hz in this dye laser. High sensitivity and high temporal and spectral resolution allow various practical applications of laser intracavity spectroscopy, such as measurements and simulations of atmospheric absorption, molecular and atomic spectroscopy, process control, isotope separation, study of free radicals and chemical reactions, combustion diagnostics, spectroscopy of excited states and nonlinear processes, measurements of gain and of spectrally narrow light emission. Intracavity absorption in single-mode lasers shows enhanced sensitivity as well, although not as high as in multimode lasers.

PACS: 42.55.Ah; 42.62.Fi

Absorption spectroscopy is one of the most important techniques for the detection and characterization of various types of matter. It is based on the measurement of the spectral extinction, by the absorber, of light transmitted through the sample. This extinction is governed by the Lambert–Beer law

$$I(\nu) = I_0(\nu) \exp[-\kappa(\nu)L] , \tag{1}$$

where $I_0(\nu)$ is the incident spectral light flux, $I(\nu)$ is the transmitted light flux, $\kappa(\nu)$ is the absorption coefficient of the sample, and L is the optical path length of the absorber. The absorption coefficient is expressed by the absorber density n and cross section σ as

$$\kappa(\nu) = n\sigma(\nu) . \tag{2}$$

The absorption signal K in the transmitted spectrum is defined as

$$K = \ln \frac{I_0}{I} . \tag{3}$$

For a small absorption signal, $\Delta I \ll I_0$,

$$K = \Delta I / I_0 \tag{4}$$

holds, with ΔI being the reduction of the light flux by the absorption.

Spectral resolution, temporal resolution, and the minimum density required for the detection of the absorber are the key parameters that determine the scope of possible practical applications of absorption spectroscopy. It is a challenge to spectroscopists to push these limits to the extremes. High spectral resolution is accomplished by the use of frequency-stabilised single-mode lasers and various Doppler-free techniques [1]. Time resolution is being improved by the application of shorter laser pulses, whose length is on the order of a few fs at present [2]. Improvements of sensitivity have mostly involved the detectivity of the light. However, the intrinsic sensitivity of the particular strategy of measurements also has actually enormous reserves.

The *detection limit* is defined as the smallest absorption coefficient $\kappa_{\min}$ detectable in the transmitted spectrum. It is characterized (i) by the *signal-to-noise ratio* in the recorded spectrum, and (ii) by the *spectral sensitivity*, which is the absorption signal per corresponding absorption coefficient. According to (1), the spectral sensitivity in conventional measurements equals the absorption path length, L. In general, we

* Corresponding author

define the spectral sensitivity as an effective absorption path length,

$$L_{\mathrm{eff}} = K/\kappa\,. \tag{5}$$

With these definitions, the detection limit is

$$\kappa_{\min} = (K)_{\min} \times (L_{\mathrm{eff}})^{-1}_{\max}\,, \tag{6}$$

where $(K)_{\min}$ is the noise-equivalent absorption signal, and $(L_{\mathrm{eff}})_{\max}$ is the maximum value of spectral sensitivity.

The noise on the detected signals of I and I_0 may be minimized by various modulation techniques for spectral recording, for example photoacoustic spectroscopy [3, 4], optothermal spectroscopy [5], and various kinds of frequency modulation spectroscopy [6, 7]. These techniques permit the recording of noise-equivalent absorption signals in the range $K_{\min} = 10^{-7}$–10^{-12}.

In this paper we shall focus on *spectral sensitivity* L_{eff}, whose inverse is the second factor in (6), which also determines the detection limit. The spectral sensitivity of absorption can be enhanced in several ways:

(i) Free propagation of light in the atmosphere [8, 9] provides up to 16 km absorption length. Such long-path measurements, however, apply only to atmospheric extinction and merely provide an average over the entire absorber length.

(ii) Multireflection cells [10, 11] allow some 100-fold extension of the effective absorber length. This factor is limited by the loss of light at the mirrors, and by the necessity of sufficient geometrical separation of the successively reflected laser beams. With 10 m base length of the cell, the effective absorption length may be at most 1 km.

(iii) Higher enhancement of the effective absorption path length is accomplished by the method of cavity ringdown spectroscopy [12]. Here, the absorber is placed inside a passive cavity, into which a short laser pulse is injected. From the measured decay time of this pulse, the absorption is derived. The effective absorption length is determined by the average number of round trips of the light, and by the cavity length L. With high-quality mirrors, 70 km has been achieved [13].

(iv) Very high spectral sensitivity is obtained by intracavity absorption spectroscopy (ICAS) with a multimode laser whose homogeneously broadened gain exceeds the absorption linewidth [14–19]. In such a multimode laser, the broadband cavity loss is compensated by the laser gain. This laser is equivalent to an undamped cavity with extremely high finesse, 10^5–10^{10}, which is limited by the perturbations of light coherence only, for example, by spontaneous emission. The emission spectrum of this laser is extremely sensitive to narrow-line absorption in the cavity thanks to the enormous effective absorption path length. The highest value recently established with a cw Rh6G dye laser is 70 000 km [20].

In this paper we present the most important results achieved by theoretical and experimental studies of the ICAS technique, and by its application. The principles of ICAS are recollected in Sect. 1. Spectral dynamics of ideal multimode lasers is introduced in Sect. 2. The high sensitivity of the laser emission spectrum to intracavity absorption (ICA) is explained in Sect. 3, and the fundamental sensitivity limit to ICA is estimated in Sect. 4. Perturbations of the ideal laser dynamics, such as quantum fluctuations, Rayleigh scattering and mode coupling, and their influence on the sensitivity and linearity of absorption measurements are discussed in Sect. 5. Full-scale fluctuations of light in individual modes take place as a result of weak mode coupling; they are analysed in Sect. 6. The prerequisites for quantitative measurements of absorption coefficients are outlined in Sect. 7. In the subsequent section, the combination of ICAS with noise reduction is inspected. This combination allows simultaneous optimization of both factors in (6), i.e. a multiplicative reduction of the detection limit. The results obtained by ICAS with different lasers, such as Nd^{3+}-doped glass laser, dye laser, Ti:sapphire laser, colour centre laser, diode laser, doped fibre laser, and optical parametric oscillator are reviewed in Sect. 9. The specific potential for enhancing the sensitivity of ICAS measurements is shown. Various practical applications of ICAS based on its high sensitivity and high temporal resolution are outlined in Sect. 10, and the ultimate spectral resolution of ICAS is discussed in Sect. 11. Finally, the application of *single-mode* lasers for ICAS is shown in comparison to multimode lasers in Sect. 12.

1 Principles of ICAS with multimode lasers

The principal features of ICAS with multimode lasers are shown in Fig. 1. The laser cavity consists of two mirrors M1 and M2 and includes a medium of broadband gain $G(\nu)$ and a sample with a narrow-line absorption spectrum $\kappa(\nu)$. The sample is either confined in an absorption cell, or just placed in an open part of the cavity. The foremost requirement for the application of multimode ICAS is that the linewidth of the absorber is smaller than homogeneous spectral broadening of the gain medium. Although the laser gain is made to compensate broadband cavity loss such as the mirror transmission, it is not affected by narrow-line ICA. The laser light passes through the absorber many times, and ICA is accumulated in its spectrum, as in a multipass cell. Additional inhomogeneous broadening of the gain is beneficial, since the spectral range for absorption measurements with a particular laser is broadened. However, if the absorber linewidth equals or even exceeds the homogeneous gain broadening, the spectral sensitivity of ICA measurements is far lower. This case is equivalent to ICAS with a single-mode laser; it will be discussed in Sect. 12. If not stated otherwise in the following, we assume that the condition of small bandwidth of absorption holds which is necessary for sensitive multimode ICAS.

For ICAS of gaseous samples whose linewidths are typically less than $0.3\,\mathrm{cm}^{-1}$, many gain media are suitable. Lasers having been successfully applied to ICAS include the Nd^{3+} glass laser [14, 15, 21, 22], dye lasers [17, 23–25], colour centre lasers [26–28], the Ti:sapphire laser [29–31], diode

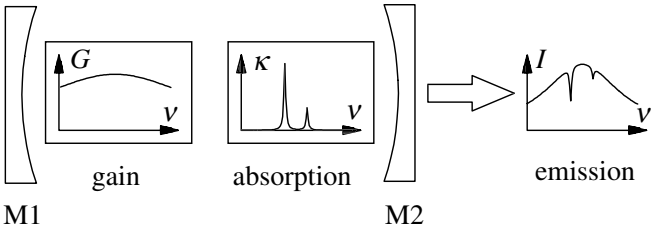

Fig. 1. Schematics of measurements of intracavity absorption

lasers [32, 33], doped fibre lasers [34], and other doped solid-state lasers. Tuning the broadband laser emission to a specific spectral region is accomplished by wavelength-selective elements in the cavity, such as a prism, a lens with chromatic aberration, or a pellicle, by using specially coated cavity mirrors, or by adjusting the parameters of laser operation and the cavity configuration.

The laser cavity has to be designed in such a way that spectrally periodic loss due to light reflection or scattering from all the optical elements in the cavity is small enough. Especially, one has to avoid optical components inside the laser with parallel or nearly parallel surfaces. Since the laser emission is so sensitive to intracavity extinction, even scattering on dust particles or imperfections of intracavity optical surfaces may be large enough to cause parasitic etalon fringes in the laser output spectrum [25, 35]. If the fringe period is comparable with the width of the absorption features in the cavity, the spectral modulation may either mask the spectral data completely or hamper a quantitative analysis. Fringes with a period that differs significantly from the absorption linewidth are harmless. In order to avoid etalon fringes the laser mirrors are preferably made of thick substrates with their back surfaces tilted by 5° to 10°. Optical windows inside the cavity have to be thick and wedged. It should be noted that even light reflected or scattered from etalons outside the cavity can re-enter the cavity through the output mirror and cause etalon fringes in the laser output. Undesirable spectrally periodic structures in the averaged emission spectrum of the laser can be reduced by periodic modulation of the positions of the critical optical elements, for example by piezoelectric elements [35, 36]. The application of a unidirectional ring laser for ICAS also reduces the spectral modulation of loss [37]. Special attention has to be paid to the orientation of birefrigent crystals in solid state lasers. The crystal axis must be oriented parallel to the optical axis, or parallel to the electrical vector of the light field in the cavity, such that the birefringence of the crystal does not contribute to spectral loss modulation [30].

The emission spectrum of the laser is typically measured with a grating spectrograph and a multichannel recorder, for example, a diode array, or a photographic plate. Usually, the recording system does not resolve individual laser modes, and the discrete spectrum of laser emission appears continuous, $I(\nu)$, as schematically shown in Fig. 1. Time-resolved spectral recording is required for calibration of the sensitivity of intracavity absorption spectra. Temporal resolution is usually obtained by pulse modulation of the pump power, for example, by an acousto-optic deflector or by an electro-optic modulator, such that the broadband laser is switched alternately above and below the laser threshold. After a preselected time interval measured from the onset of the broadband laser oscillation, the laser output is deflected by a second acousto-optic deflector for a short time interval on the entrance slit of the spectrograph for detection [38]. Alternatively, the spectrum is recorded continuously as a function of time by a mechanical streak camera [21, 39], or by an optical multichannel analyser with sufficient time resolution [30]. Fourier-transform interferometry may also allow for time-resolved spectral recording of laser emission and ICA [40, 41]. This technique is especially useful in the infrared spectral range where conventional diode arrays would be either not available, or very expensive, and of poor quality.

The application of a monochromator [42] and a Fabry–Pérot etalon [43] for stepwise recording the spectrum of laser emission forfeits parallel data acquisition: the recording is sequential, and instabilities of the total laser power are transformed into equivalent spectral noise. With parallel spectral recording, – i.e. by polychromator and diode array – instabilities of the total laser power are not harmful.

An alternative way for recording broadband IR laser emission is up-conversion of IR light by mixing it in a nonlinear crystal with monochromatic light [44]. The wavelength of the up-converted light is adjusted by properly setting the wavelength of the narrow-band laser. In this way, the IR emission spectrum of the laser can be read out in the visible range by conventional diode arrays. Moreover, the application of a pulsed monochromatic laser for up-conversion acts as a time gate and allows for time-resolved spectral recording [45].

Nondispersive techniques such as fluorescence [17], photoacoustic [46], or optogalvanic spectroscopy [47] may be applied to the recording of intracavity absorption as well. In these variants, the same types of gases to be detected inside the laser cavity have to be contained at high concentration in the external fluorescent, photoacoustic, or optogalvanic cells, respectively. ICA selectively quenches the broadband light and makes the corresponding signal of the external cell decrease.

2 Spectral dynamics of multimode lasers

Many properties of multimode lasers and, in particular, the temporal evolution of their emission spectrum and the response to intracavity absorption are satisfactorily described by rate equations for the *mean values* of the photon numbers M_q in the laser mode q, and for the laser inversion N [19]. In this section we neglect, for simplicity, the stochastic nature of spontaneous emission, and the wave nature of the light, as well as the coupling of laser modes – except by their common gain. We assume that the gain is homogeneously broadened only, and that the laser operates in the ideal four-level configuration: the relaxation of the pump level to the upper laser level, and of the lower laser level to the ground level is assumed to be very fast compared with the relaxation from the upper to the lower laser level. This situation appears, for example, with dye lasers. The rate equations for such a laser are

$$\dot{M}_q = -\gamma M_q + B_q N(M_q + 1) - \kappa_q c M_q \,, \tag{7}$$

$$\dot{N} = P - AN - N \sum_q B_q M_q \,. \tag{8}$$

Here, γ is the broadband cavity loss, κ_q is the absorption coefficient of intracavity absorption at the q-th axial laser mode, c is the velocity of light, P is the pump rate, and A is the rate of spontaneous decay of the upper laser level. Laser inversion equals the population N of the upper laser level. Equation (7) includes the mean value of the rate of spontaneous emission $B_q N$ [48], which is considered the only perturbation of laser dynamics in this approximation. The homogeneously broadened laser gain, expressed as a rate B_q of induced emission per one inverted dye molecule and per one photon in mode q,

is approximated by the Lorentzian profile

$$B_q = \frac{B_0}{1 + \left(\frac{q-q_0}{Q}\right)^2}\,, \tag{9}$$

with the frequency variable scaled in units of the mode numbers, $q = 2L/\lambda_q$. Here, L is the length of the cavity, and λ_q is the wavelength of the light in mode q. The maximum gain at the central mode q_0 is B_0, and the spectral width of the gain is Q (HWHM). The laser gain B_0 is the product of the Einstein coefficient for stimulated emission, B, and a factor that depends upon the particular geometry of the laser beam in the cavity.

Let us consider the spectral dynamics of a Rh6G dye laser with typical parameters, such as $A = 1.7 \times 10^8\ \mathrm{s}^{-1}$, $B_0 = 10^{-2}\ \mathrm{s}^{-1}$, $\gamma = 1.5 \times 10^6\ \mathrm{s}^{-1}$, i.e., 1% loss per round trip, the spectral width of the gain $Q = 2.5 \times 10^5$, and $L = 1$ m. After the pump power is switched on at $t = 0$, the laser dynamics extends over four time regimes, characterized by subsequent increasing saturation of different variables: (i) the laser inversion N, (ii) the total photon number $M = \sum M_q$, and (iii) the photon numbers M_q in individual laser modes, such that finally (iv) the spectral output is stationary.

The laser dynamics in the first two regimes is analysed under the assumption that the dye laser operates near the maximum of its spectral gain, and that the gain is approximately constant over all m oscillating modes. Under these conditions, rate (7) and (8) can be summed over q:

$$\dot{M} = -\gamma M + B_0 N(M + m)\,, \tag{10}$$

$$\dot{N} = P - AN - B_0 NM\,. \tag{11}$$

The *first time regime*, $t < t_{\mathrm{th}}$, is characterized by the growth of laser inversion as

$$N = \eta N_{\mathrm{th}} \left(1 - \mathrm{e}^{-At}\right)\,. \tag{12}$$

Here, η is the normalized pump rate $\eta = P/P_{\mathrm{th}}$, with $P_{\mathrm{th}} = AN_{\mathrm{th}}$ being the threshold pump rate, and $N_{\mathrm{th}} = \gamma/B_0$ being the threshold inversion. In this time regime the inversion is smaller than at the laser threshold, $N < N_{\mathrm{th}}$, and $M \cong 0$. The duration of the build-up of laser inversion is about $1/\eta A$.

The *second time regime*, $t_{\mathrm{th}} < t < t_M$, is characterized by the saturation of laser inversion at the intermediate quasi-stationary level $N = \eta N_{\mathrm{th}}$. The total photon number in the laser cavity grows exponentially as $\exp[(\eta - 1)\gamma t]$, until the inversion is depleted to its final stationary value $N = N_{\mathrm{th}}$ at $t = t_M$. At that time the total photon number approaches its stationary value

$$M^{\mathrm{s}} \cong \frac{A}{B_0}(\eta - 1)\,. \tag{13}$$

The numerical solutions of (10) and (11), for $\eta = 2$, are shown in Fig. 2. The first time regime extends over 4 ns, and the second one over 80 ns.

During $t > t_M$, the total photon number in the laser cavity M, and the laser inversion N, keep their stationary values, M^{s} and N^{s}, respectively. However, the spectral distribution of the photon numbers among laser modes still continues to vary. This spectral dynamics can be obtained by solving (7) and (8). Figures 3 and 4 demonstrate, in 3-D representation, spectrally

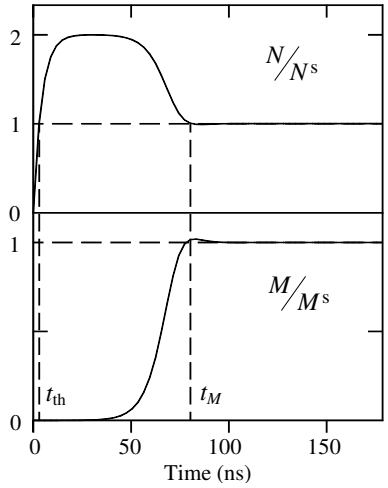

Fig. 2. Transient dynamics of the inversion N and of the total photon numbers M normalized by their stationary values N^{s} and M^{s} in the cavity of a Rh6G dye laser calculated according to (10) and (11)

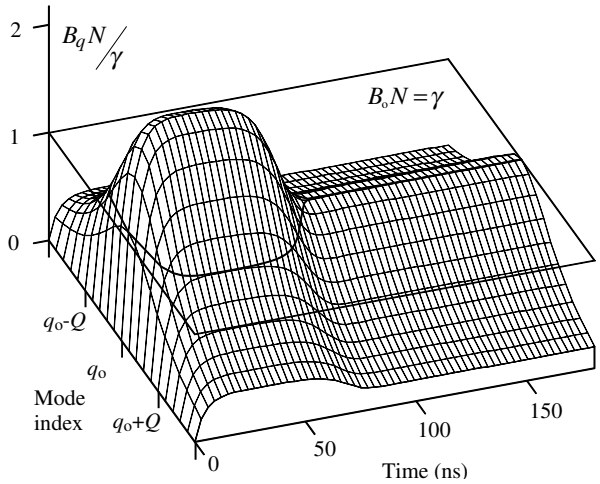

Fig. 3. Transient dynamics of the gain, B_qN, calculated for the modes q of a Rh6G dye laser at pump rate $\eta = 2$. B_0 is the maximum gain at the central mode q_0, Q is the spectral width of the gain, and γ is the cavity loss

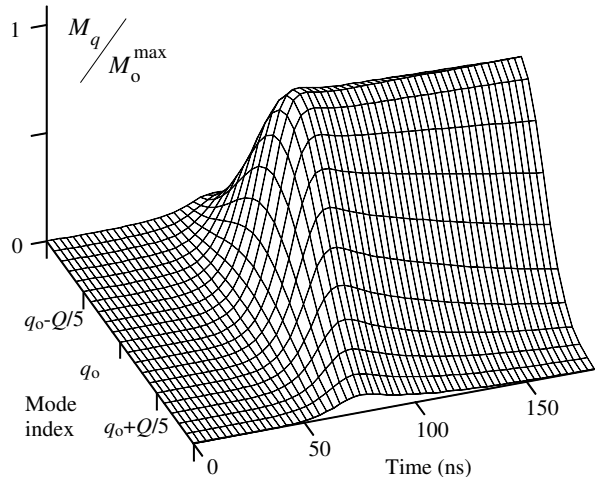

Fig. 4. Transient dynamics of the emission spectrum, calculated for the Rh6G dye laser, as in Fig. 3. M_q is the photon number in mode q that is normalized by the maximum value $M_0^{\max}$ of photon number in the central mode

and temporally resolved numerical solutions obtained for the normalized inversion $N/N_{\rm th}$ and photon numbers $M_q/M_0^{\rm max}$ in the laser modes. Laser parameters and time scale are as in Fig. 2. Figure 3 shows the spectral dynamics of the laser gain: The horizontal plane $B_0N = \gamma$ represents the level of inversion required for compensation of the cavity loss. The inversion above this plane represents positive gain for the indicated laser modes. Since the inversion, in the second time regime, is twice as large as the threshold inversion of the central mode, laser emission grows exponentially within the spectral range where the gain assumes at least half its maximum value, i.e. within its full spectral width, $2Q = 5 \times 10^5$. Figure 4 demonstrates this growth in the central part of the emission spectrum.

Figure 3 shows that laser inversion compensates the cavity loss at $t > t_M$ only for the central mode. Uncompensated loss of other modes results in decaying emission. Since the total laser power stays constant at that time (see Fig. 2), redistribution of the power from the distant modes to the central modes takes place. This "spectral narrowing", or "spectral condensation", of the laser emission spectrum represents the *third time regime* of the spectral dynamics. Let us assume, for a moment, that intracavity absorption is absent. With spontaneous emission neglected, the photon number in mode q,

$$M_q(t) = M^{\rm s}\frac{\sqrt{\gamma t/\pi}}{Q}\exp\left[-\left(\frac{q-q_0}{Q}\right)^2\gamma t\right], \tag{14}$$

is derived from (7)–(9). This transient spectrum has Gaussian shape with the width (HWHM)

$$\Delta q(t) = Q\sqrt{\frac{\ln 2}{\gamma t}}\,. \tag{15}$$

The light emission has been numerically calculated from (7)–(9) and is shown, vs. mode index and time, in Fig. 5 for up to 250 s time of evolution. The pump rate is $\eta = 1.3$, and the spectral interval is 100 times smaller than the one in Fig. 4. The third time regime, representing spectral condensation, extends until some 10 s. The subsequent saturation of the spectral dynamics during the final temporal evolution is caused by spontaneous emission.

Figure 6 shows the photon number M_0 in the central mode q_0 as a function of time. The logarithmic scale covers almost three orders of magnitude, and the time scale more than 6 orders of magnitude. As expected from (14), the initial growth of the light power varies as the square root of time. The spectral saturation time $t_{\rm s}^0$, required for reaching stationary emission in the central mode, is defined from the crossing of the straight line of initial growth, and the stationary value of the photon number. The data in Fig. 6 yield $t_{\rm s}^0 = 9$ s. Figures 4 through 6 show that the third time regime, including the spectral redistribution of laser emission at constant total power, extends over 8 orders of magnitude, i.e. from $t_M \cong 80$ ns, to $t_{\rm s}^0 \cong 10$ s.

At $t > t_{\rm s}^0$, a *fourth time regime* of the spectral dynamics emerges. It is characterized by a stationary light distribution, $M_q^{\rm s}$, which is derived from (7)–(9) including spontaneous emission:

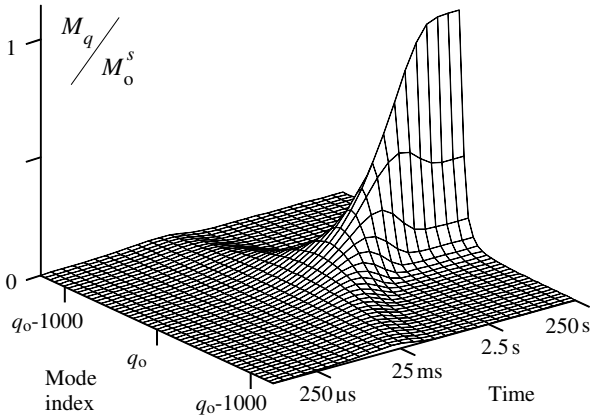

Fig. 5. Transient dynamics of the emission spectrum, calculated for the Rh6G dye laser at pump rate $\eta = 1.3$; the time scale is compressed by 10^9, and the spectral scale is expanded by 10^2 as compared to Fig. 4. Photon numbers M_q are normalized to the stationary photon number $M_0^{\rm s}$ in the central mode

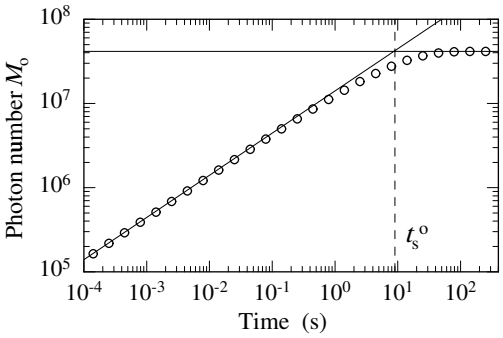

Fig. 6. Photon number M_0 in the central mode, vs. duration of laser emission, in the peak of the spectrum in Fig. 5; $t_{\rm s}^0$ is the spectral saturation time of emission

$$M_q^{\rm s} = \frac{M_0^{\rm s}}{1 + M_0^{\rm s}\left(\frac{q-q_0}{Q}\right)^2}\,. \tag{16}$$

Here, $M_0^{\rm s}$ is the stationary photon number in the central mode q_0. After normalization by $\sum M_q^{\rm s} = M^{\rm s}$, and using (13), we obtain

$$M_0^{\rm s} = \left(\frac{M^{\rm s}}{\pi Q}\right)^2 = \frac{A^2(\eta-1)^2}{\pi^2 B_0^2 Q^2}\,. \tag{17}$$

According to the above definition, the spectral saturation time of the *emission* into the central mode is obtained from (14) and (17), assuming $M_0(t_{\rm s}^0) = M_0^{\rm s}$, as

$$t_{\rm s}^0 = \frac{A^2(\eta-1)^2}{B_0^2 Q^2 \pi^3 \gamma} = \frac{M_0^{\rm s}}{\pi\gamma}\,. \tag{18}$$

Substituting the parameters of the Rh6G dye laser (with $\eta = 1.3$) we obtain $t_{\rm s}^0 = 9$ s, which agrees with the value resulting from the numerical data that are plotted in Fig. 6.

The stationary laser spectrum in (16) has Lorentzian shape, with the width (HWHM)

$$\Delta q^{\mathrm{s}} = \frac{Q}{\sqrt{M_0^{\mathrm{s}}}} = \frac{\pi B_0 Q^2}{A(\eta - 1)} \,. \tag{19}$$

The stationary emission bandwidth calculated with the laser parameters of Fig. 5 is remarkable: $\Delta q^{\mathrm{s}} = 39$ modes. It has been conjectured that one laser mode only survives owing to mode competition if the gain is homogeneously broadened [49]. This conclusion would indeed hold if spontaneous emission were considered very weak and, therefore, meant to be neglected. Then, the condensation of the laser spectrum according to (14) would continue till finally one laser mode survived. However, spontaneous emission, even if much smaller than induced emission, cannot justifiably be neglected since it limits the spectral condensation, and defines the spectral saturation time, the width of the stationary emission spectrum, and the spectral width of individual laser modes [50].

Stationary inversion, N^{s}, derived from (7) is determined by the mode with the smallest net loss. In the above simple model, it is the central mode, and

$$N^{\mathrm{s}} = \frac{\gamma}{B_0} \left(1 - \frac{1}{M_0^{\mathrm{s}}} \right) \,. \tag{20}$$

This expression shows that the laser gain $B_0 N^{\mathrm{s}}$ in the stationary state is always exceeded by the cavity loss γ, even for the strongest mode: the loss in the cavity is compensated by the laser gain, *and* by spontaneous emission.

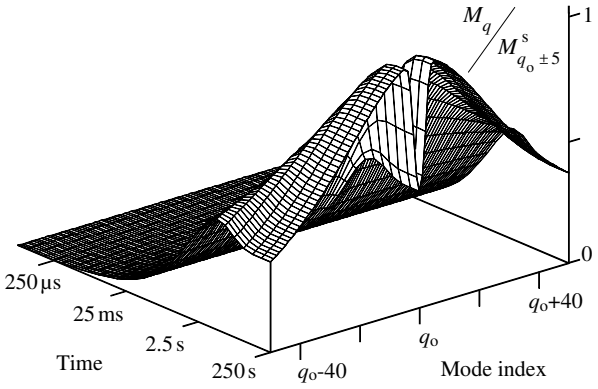

Fig. 7. Transient dynamics of the emission spectrum calculated for the Rh6G dye laser, as in Fig. 5, but with ICA line of absorption coefficient, $\kappa = 1.2 \times 10^{-12}\,\mathrm{cm}^{-1}$ at $q = q_0$. Photon numbers M_q are normalized by the stationary photon number in the strongest modes, $q_0 \pm 5$

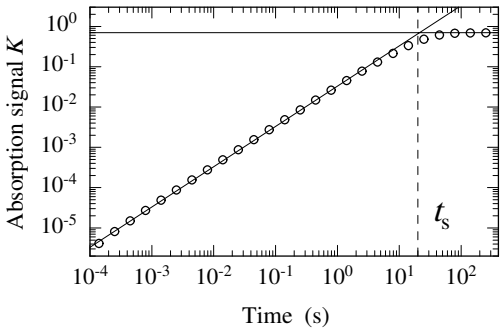

Fig. 8. Absorption signal K in the mode q_0, vs. duration of laser emission, calculated from the spectrum in Fig. 7; t_{s} is the spectral saturation time of absorption

3 Sensitivity to intracavity absorption

Narrow-band intracavity absorption κ_q causes additional loss in the corresponding laser modes and, as a consequence, exponential decay of the photon numbers as compared with the undisturbed laser mode. The solution of rate equations (7) and (8) in the third time regime, (14), is modified by ICA to yield

$$M_{q,\kappa}(t) = M_q(t) \exp(-\kappa_q c t) \,, \tag{21}$$

which is equivalent to the Lambert–Beer law, (1), where the absorption path length is substituted by the effective absorption path length $L_{\mathrm{eff}} = ct$.

In order to demonstrate the effect of ICA on the spectral laser dynamics and the stationary state, we have numerically solved the rate equations (7)–(9), with the inclusion of a weak absorption line. The absorption coefficient has been set to $\kappa_0 = 1.2 \times 10^{-12}\,\mathrm{cm}^{-1}$, and its spectral width to $\Delta q = 2$ (HWHM) in the centre of the gain spectrum. Such an absorption line corresponds to the Doppler-broadened (T = 20 K) transition $3S_{1/2} \rightarrow 3P_{3/2}$ in sodium with the density $0.05\,\mathrm{cm}^{-3}$. The modified spectral laser dynamics is shown in Fig. 7, where the laser parameters are the same as in Fig. 5, except for ICA. In order to spectrally resolve the absorption line, the frequency scale in Fig. 7 is expanded again, such that only 100 central modes are left over. Indeed, Fig. 7 shows the absorption signal in the centre of the emission spectrum. This signal initially increases with the duration of laser emission, and finally saturates to its stationary spectral shape. According to (3) the value of the absorption signal K_q in mode q is

$$K_q = \ln \frac{M_q}{M_{q,\kappa}} \,, \tag{22}$$

where the number of photons in mode q is $M_{q,\kappa}$ in the presence of ICA, and M_q in the absence. The value M_q may be estimated by determining the number of photons in one of the neighbouring modes that is not modified by the absorption. As a result, the difference of the net loss in the cavity at the wavelengths of the corresponding laser modes is derived.

Figure 8 shows the absorption signal K_q of the mode q_0, due to ICA, corresponding to Fig. 7. The absorption signal grows linearly, with the duration of laser emission during the initial stages of laser operation, as expected from (21) and (22),

$$K_q = \kappa_q c t \,. \tag{23}$$

The absorption signal is estimated by taking the photon numbers in the mode q_0 for $M_{q,\kappa}$, and in mode $q_0 + 5$ for M_q. Since the mode $q_0 + 5$ still suffers the residual ICA absorption $0.14\kappa_0$, and its gain is smaller by $0.05\kappa_0$, the resulting absorption signal corresponds to the loss difference $\kappa = \kappa_0 - \kappa_5 = 1 \times 10^{-12}\,\mathrm{cm}^{-1}$. The solid line in Fig. 8, an extrapolation of the linear fit of K_q in the initial stage, shows the

temporal evolution of this absorption signal, expected with the linear dependence of (23), which holds up to 20 s. Afterwards, the absorption signal saturates to its stationary value.

4 The fundamental limit of sensitivity

The mean stationary mode distribution of the photon numbers in the laser with ICA is calculated analytically, like (16), from (7) and (20) at $\dot{M} = 0$:

$$M^{\mathrm{s}}_{q,\kappa} = \frac{M^{\mathrm{s}}_q}{1 + \frac{c\kappa_q M^{\mathrm{s}}_q}{\gamma}} \,. \tag{24}$$

With this result, the stationary absorption signal in mode q is calculated from (22) as

$$K^{\mathrm{s}}_q = \ln\left(1 + \frac{\kappa_q c M^{\mathrm{s}}_q}{\gamma}\right) . \tag{25}$$

When intracavity absorption is weak, such that $K^{\mathrm{s}} \ll 1$, (25) becomes

$$K^{\mathrm{s}}_q \cong \frac{\kappa_q c M^{\mathrm{s}}_q}{\gamma} \,. \tag{26}$$

Extrapolation of the linear time dependence in (23) to the stationary solution in (26) yields the spectral saturation time t_{s} of the *absorption signal*,

$$t_{\mathrm{s}} = \frac{K^{\mathrm{s}}_q}{c\kappa_q} = \frac{M^{\mathrm{s}}_q}{\gamma} \,, \tag{27}$$

which determines the effective absorption length,

$$L_{\mathrm{eff}} = ct_{\mathrm{s}} = \frac{cM^{\mathrm{s}}_q}{\gamma} \,, \tag{28}$$

achievable in the detection of ICA under cw operation. This quantity characterizes the laser dynamics, not the measured absorption line, and is the *fundamental sensitivity limit*. It is the same for all absorption lines small enough and situated in the same part of the laser output spectrum. Note that (27) can be used for the calculation of t_{s} in order to evaluate the absorption in the laser spectrum. In contrast, t^0_{s} of (18) is the spectral saturation time of *emission* in the central laser mode. According to (18) and (27), the spectral saturation times of emission and absorption at the central mode $q = 0$ are related, but differ: $t_{\mathrm{s}} = \pi t^0_{\mathrm{s}}$.

At the central mode, the effective absorption length, according to (17) and (28), is

$$L_{\mathrm{eff}} = \frac{A^2(\eta-1)^2 c}{\pi^2 B_0^2 Q^2 \gamma} = G(\eta-1)^2 \,, \tag{29}$$

where $G = (A/\pi BQ)^2 c/\gamma$ is the effective absorption length at the pump rate $\eta = 2$, which is a specific value for the laser used. The duration of laser emission required to exploit this sensitivity is $t_{\mathrm{s}} = L_{\mathrm{eff}}/c$. With the Rh6G dye laser in the above example, $G = 9.4 \times 10^7$ km. At $\eta = 1.3$, we expect to reach $L_{\mathrm{eff}} = 8.37 \times 10^6$ km, which is 20 times the distance from Earth to Moon. The corresponding spectral saturation time is $t_{\mathrm{s}} = 28$ s. Estimates by (29) are valid for weak absorption signals, for mirrors with a flat spectral profile of reflection, and with no additional selective elements in the cavity reducing the emission bandwidth.

Strong ICA, such as in Figs. 7 and 8, modifies the emission spectrum, and (17) and (26) do not hold any more. The different photon numbers in laser modes at the centre and on the wing of an absorption line saturate after different times. An estimate of sensitivity, by (28), for a strong absorption line should involve an *effective* photon number [51],

$$M_{\mathrm{eff}} = M^{\mathrm{s}}_q \frac{K^{\mathrm{s}}_q}{\exp(K^{\mathrm{s}}_q) - 1} = M^{\mathrm{s}}_{q,\kappa} \frac{K^{\mathrm{s}}_q}{1 - \exp(-K^{\mathrm{s}}_q)} \,, \tag{30}$$

which is an intermediate value between the photon numbers in the compared modes. The spectral saturation time determined in Fig. 8 from the results of numerical calculations is about 20 s. This result complies well with the value of the effective photon number in this line, $M_{\mathrm{eff}} = 0.7 M_q$.

Equation (29) allows the estimation of the fundamental limit of sensitivity to ICA obtainable with other lasers. For instance, with a Ti:sapphire laser [30] $G = 1.3 \times 10^9$ km ($A = 3 \times 10^5\ \mathrm{s}^{-1}$, $B_0 = 2 \times 10^{-6}\ \mathrm{s}^{-1}$, $\gamma = 1.5 \times 10^6\ \mathrm{s}^{-1}$, $Q = 6 \times 10^5$, $L = 1.85$ m), and with GaAlAs diode laser [32] $G = 2.5 \times 10^2$ km ($A = 10^9\ \mathrm{s}^{-1}$, $B_0 = 10\ \mathrm{s}^{-1}$, $\gamma = 10^9\ \mathrm{s}^{-1}$, $Q = 3.5 \times 10^4$, $L = 0.7$ m).

5 Perturbations of laser dynamics

The fundamental sensitivity limit is expected to grow with the pump rate according to (29). However, experiments show that the sensitivity of various lasers does not obey this prediction. Only diode lasers have proven so far to show this fundamentally limited sensitivity [32, 52]. Figure 9 [53] shows the sensitivity to ICA of various lasers measured as a function of pump power. The sensitivity is expressed as the effective length of absorption, L_{eff}, determined from the spectral saturation time t_{s} that was recorded in experiments. In contrast to diode lasers, solid-state lasers, such as Ti:sapphire [29, 30] and doped fibre lasers [34, 54], show almost no dependence of

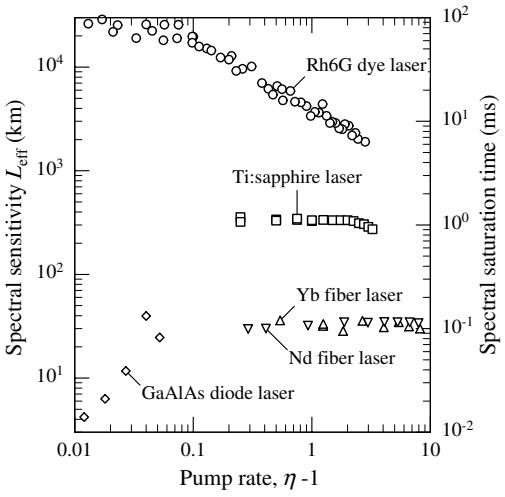

Fig. 9. Sensitivity to intracavity absorption, L_{eff}, and spectral saturation time t_{s} measured with various lasers, vs. pump rate

their sensitivity upon the pump rate. Moreover, the sensitivity to ICA achieved with dye lasers *decreases* with the pump rate [55, 56].

According to the observed performance we conclude that the sensitivity of multimode lasers to ICA is limited by qualitatively different kinds of perturbation of the laser dynamics. The effect of these perturbations can be analysed by including individually modelled rates X_q of perturbation of the laser emission in the rate (7),

$$\dot{M}_q = (-\gamma + B_q N - \kappa_q c) M_q + X_q \,. \tag{31}$$

If no rate of perturbation exceeds that of spontaneous emission, $X_q = B_q N$, according to (7).

The mean stationary spectral distribution of laser emission is obtained from (31) at $\dot{M} = 0$,

$$M^{\mathrm{s}}_{q,\kappa} = \frac{X_q}{\gamma - B_q N^{\mathrm{s}} + \kappa_q c} \,. \tag{32}$$

With this result the stationary absorption signal in mode q is calculated from (22) as

$$K^{\mathrm{s}}_q = \ln\left(1 + \frac{\kappa_q c}{\gamma - B_q N^{\mathrm{s}}}\right) \,. \tag{33}$$

The stationary inversion N^{s} is determined by the laser modes with maximum net gain; it is calculated from (31) at $\kappa_q = 0$:

$$N^{\mathrm{s}} = \frac{\gamma}{B_0} - \frac{X_q}{B_0 M^{\mathrm{s}}_0} \,. \tag{34}$$

When intracavity absorption is weak, such that $K^{\mathrm{s}} \ll 1$, (33) becomes

$$K^{\mathrm{s}}_q \cong \frac{\kappa_q c M^{\mathrm{s}}_q}{X_q} \,. \tag{35}$$

Extrapolation of the linear dependence in (23) to the stationary solution in (35) yields the characteristic time of spectral saturation, $t_{\mathrm{s}} = M^{\mathrm{s}}_q / X_q$, and the effective absorption length

$$L_{\mathrm{eff}} = \frac{c M^{\mathrm{s}}_q}{X_q} \,. \tag{36}$$

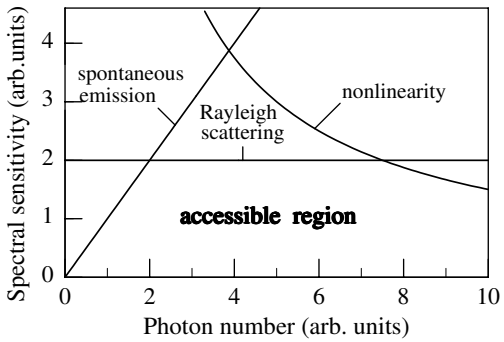

Fig. 10. Limitation of ICAS sensitivity by three mechanisms of pertubation included in the model. The range of parameters accessible in the measurements is indicated

The sensitivity limit of absorption measurements expressed in (36) depends upon the rate of the particular perturbation of the laser light, X_q. We consider now three types of perturbations, whose effects depend in qualitatively different ways on the strength of the intracavity light, and whose respective dominance is schematically shown in Fig. 10.

5.1 Spontaneous emission

The perturbation by spontaneous emission, $X_q = B_q N$, is fundamental and present in all lasers. It has been included before even in the simplified model. Under stationary laser operation $B_q N^{\mathrm{s}} \cong \gamma$, and the sensitivity to ICA grows with the pump rate, which complies well with the performance of diode laser (Fig. 9). Their sensitivity rises with the pump rate, at least close to the threshold, $\eta < 1.05$ [52]. However, their achieved sensitivity is poorer than that of other laser types: the high intrinsic loss and low output power of diode lasers are responsible for their low sensitivity. In this type of laser, the dominance of spontaneous emission is brought about by the high internal loss in the laser diode. Other lasers show far smaller loss and, therefore, less gain and a higher fundamental limit of their sensitivity. The specific perturbation of coherence by spontaneous emission is enhanced in lasers whose modes are non-orthogonal [57]. This enhancement is rather strong in lasers with unstable cavities.

5.2 Rayleigh scattering

Rayleigh scattering of the laser light off local fluctuations of density and temperature in a dense gain material shifts the frequency and the phase of a fraction of the light in the cavity modes. Since the frequency shift is small, the scattered light remains in the same mode and disturbs the phase coherence of the light [58]. The rate of perturbation of the laser is expressed by the fractional rate of scattered light $X_q = R M^{\mathrm{s}}_q$, with R being the rate of scattering into the laser mode. According to (36), the spectral sensitivity,

$$L_{\mathrm{eff}} = c/R \,, \tag{37}$$

is now independent of the pump power. Whenever Rayleigh scattering is assumed to be the dominant perturbation, the sensitivity to ICA is not expected to vary with the pump rate and photon numbers in laser modes, as shown in Fig. 10. Such a performance has been observed with solid-state lasers, for example, Ti:sapphire and fibre lasers that have a long and dense gain medium. In a good fibre, the loss by Rayleigh scattering at 1.1 μm is about $\delta = 0.4$ dB/km [59]. If we assume that all the scattered light acts as perturbation, then $R \cong 0.23 \delta c = 2.8 \times 10^4\,\mathrm{s}^{-1}$. According to (37) the spectral sensitivity amounts to $L_{\mathrm{eff}} = 1/0.23\delta = 11$ km. If the fibre fills only part of the cavity length, the spectral sensitivity is higher, as the rate of Rayleigh scattering per round trip of the laser is cut down. The spectral sensitivity of Nd^{3+}- and Yb^{3+}-doped fibre lasers to ICA is found to be in the range 10–130 km [34, 54] (see also Fig. 9). These data prove the dominance of Rayleigh scattering on the spectral sensitivity of fibre lasers. A short gain medium in the cavity helps in general: A typical Ti:sapphire laser whose gain medium

fills a smaller fraction of the cavity length, as compared with a fibre laser, shows respectively higher sensitivity.

The effect of Rayleigh scattering in a rhodamine 6G dye laser has been simulated by re-injection of part of the frequency-shifted laser light into the cavity [50]. The strength of this optical feedback is controlled by making the light pass filters of suitable optical density. Increased feedback has been shown to reduce the sensitivity and broaden the emission bandwidth. This observation confirms Rayleigh scattering as a potentially effective perturbation of laser coherence.

5.3 Nonlinear susceptibility

The highest sensitivity to ICA has been obtained so far with a cw dye laser [20, 60, 61]. The width of the dye jet takes such a small portion of the cavity that the effect of Rayleigh scattering is almost absent. Now, the sensitivity is limited by one of various *third-order nonlinearities*. This perturbation may be expressed by $X_q = D(M_q^s)^2$, where D is a field-independent function of the relevant nonlinear susceptibility [56], if the mode amplitudes are considered uncorrelated. According to (36), the spectral sensitivity *decreases* with increasing light power in the mode,

$$L_{\text{eff}} = c/DM_q^s\,, \tag{38}$$

which is schematically shown in Fig. 10. The variation of the spectral saturation time upon the pump rate is weaker, however, than that upon the photon number in the mode, since the emission bandwidth also grows with the pump rate. The photon number in the central mode is calculated, as a function of the pump rate, from (13) and (14) by setting $t = t_s^0$. We assume that relation $t_s^0 = t_s/\pi$, derived in Sect. 4 in the case of perturbation by spontaneous emission only, holds. Substituting $t_s = 1/DM_q^s$ one derives the spectral sensitivity from (38) as function of the pump-rate excess $\eta - 1$,

$$L_{\text{eff}}^0 = c\left(\frac{\pi^2 B_0^2 Q^2}{A^2 D^2 \gamma}\right)^{1/3} \frac{1}{(\eta-1)^{2/3}}\,. \tag{39}$$

The actually measured sensitivity is assumed to deviate from this equation since (14) is valid only under the idealizing approximation that the net cavity gain equals the single-pass spectral gain. However, the effective gain turns out modified by spectrally selective reflection of the laser mirrors, and by atmospheric ICA lines. Moreover, mode amplitudes might be correlated by nonlinear coupling. In fact, the spectral sensitivity of the dye laser in Fig. 9 decreases with increasing pump rate at $\eta > 1.05$. At lower levels of the pump rate the sensitivity saturates to the constant value $L_{\text{eff}} \cong 30\,000$ km. This value is three orders of magnitude higher than the sensitivity obtained with a fibre laser, and two orders of magnitude higher than that of a Ti:sapphire laser. This enormous difference of sensitivities corresponds to different filling factors of the gain medium in the cavity which are 10%–50% in a fibre laser, 1%–2% in a Ti:sapphire laser, and 0.005% in a dye laser.

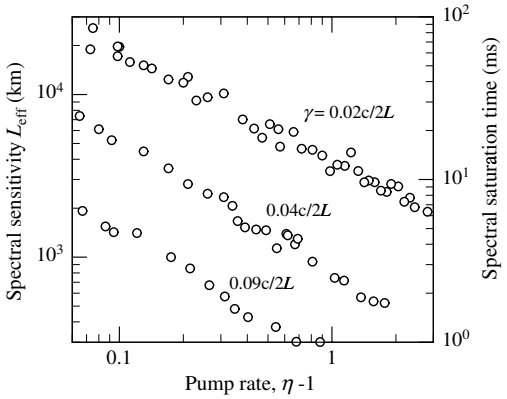

Fig. 11. Sensitivity of a cw dye laser, L_{eff}, and spectral saturation time t_s versus pump rate, $\eta - 1$, at different values of cavity loss γ. The length of the laser cavity is L

Figure 11 shows data of the spectral saturation time, measured in a Rh6G dye laser, versus the pump-rate excess, in the range $0.06 \le (\eta - 1) \le 3$, for 2%, 4%, and 9% loss per cavity round trip. The cavity loss has been varied by the mirror transmission. The spectral sensitivity varies upon the pump rate as $(\eta - 1)^x$, with x in the range from -0.6 to -0.8, which reasonably agrees with (39).

5.4 Mode coupling

Particularly harmful to the attainment of good spectral sensitivity is any interaction that efficiently couples the laser modes. Major contributions to mode coupling in a solid-state or liquid laser arise from the nonlinearities of the active medium and the saturated gain. An incident pair of light waves of different frequencies generates a material excitation at its beat frequency; in turn, the material excitation interacts with each of the incident waves and induces dielectric polarizations whose frequencies are shifted away from that of the incident waves by the beat frequency. This coupling generates four-wave mixing of the light. If only two light modes are involved, the four-wave mixing is degenerate and gives rise to spatial hole burning. In a multimode laser, however, there are many light waves of different frequencies corresponding to the longitudinal cavity modes. Each pair of these light waves reads out material excitations, created by *all other* pairs of light waves with the same beat frequency. Hence, stimulated scattering in a multimode laser entails degenerate *and* nondegenerate four-wave mixing.

The most important nonlinearities governing the dynamics of multimode dye lasers and reducing their sensitivity to ICA are mode coupling by four-wave mixing via *stimulated Brillouin scattering* (SBS) [56, 62, 63], and via *population pulsations* (PP) in the gain medium [63–68]. These nonlinearities have been modelled using various levels of simplification: SBS was described as incoherent scattering of photons between cavity modes [56, 62], four-wave mixing by PP only in the degenerate case of spatial hole burning [17, 69–71]. Later it was shown that the effect of spatial hole burning *alone* does not match, in a cw dye laser with a thin jet, even the sensitivity-reducing effect of spontaneous emission [25], whereas either the additional consideration of quantum fluctuations [72], or the inclusion of temporal PP gives rise to substantial loss of sensitivity [66]. All these models, marred by incomplete accounting of four-wave mixing, underestimate the actual effect of mode coupling on the sensitivity of dye lasers to ICA.

Adequate modelling the effect of mode coupling on the multimode laser dynamics requires full numerical evaluation of four-wave mixing via SBS and PP including light phases and quantum fluctuations [63]. This laser model makes use of complex light amplitudes, a_q, such that nonlinear scattering is described in terms of general four-wave mixing driven by the intermode beat notes, and of phase-dependent scattering S_r [63, 73]. Thus, any possible mechanism, in particular SBS, PP, and the effects of electronic nonlinearities, is represented. For simplicity we consider a class A laser, for example a dye laser, where inversion and polarization can be adiabatically eliminated on the long time scale of the evolution of laser light. The equation of motion of the light amplitudes in a multimode dye laser is

$$\dot{a}_q = \frac{1}{2}(B_q N - \gamma - \kappa_q c)a_q + f_q + \frac{1}{2}\sum_r S_r a_{q+r} \sum_p R_{p-q,r} a^*_{p+r} a_p \,. \tag{40}$$

Here, $R_{p,q,r}$ is the spatial correlation of laser modes p, q, and r. Quantum fluctuations are described by the Langevin force f_q that is normalized as

$$\langle f_q(t)\rangle = 0\,;\ \langle f^*_p(t)\, f_q(t')\rangle = \gamma\delta(t-t')\delta_{p,q}\,, \tag{41}$$

such that (40) is transformed to (7) at $S = 0$ by setting $M_q = a_q a^*_q$. The scattering function, defined for the dominant population pulsations [63] is

$$S_r^{(\mathrm{PP})} = \frac{\gamma B_0}{\eta A - \mathrm{i}\omega_r}\,. \tag{42}$$

Numerical simulations have revealed characteristics of the multimode laser dynamics that derive from population pulsations: the strength of the pulsations varies in proportion with the cavity loss, as expected from (42), the power in individual laser modes is low-frequency modulated, and the intermode beat notes become suppressed. The appearance of these phenomena has been confirmed by recording the spectral laser dynamics of a cw Rh6G dye laser [63, 73]. Figures 9 and 11 show the reduction of the sensitivity to ICA, measured with this laser, as the pump rate *or* the cavity loss increases. On the other hand, simulations performed of the laser dynamics with perturbation by mere SBS, show *no* dependence upon the cavity loss. This result proves that the dominant nonlinearity in a Rh6G dye laser of the typical parameter values listed in Sect. 2 is PP. In a unidirectional ring laser this nonlinearity is smaller than that of a standing wave laser with the same parameters. However, the additional optical elements required for the achievement of unidirectional propagation increase the cavity loss and overall PP. As a result, the perturbations by four-wave mixing in a standing-wave laser and in a unidirectional ring laser in fact are comparable in strength.

The parametric variation of the effects of four-wave mixing, spontaneous emission, and Rayleigh scattering in a cw dye laser may be plotted in a two-dimensional diagram as in Fig. 12. It separates the regions, in parameter space of loss and pump rate, where a particular phenomenon is responsible for the limitation of sensitivity of the laser to ICA. These regions are identified from the results of the computer simulations, taking into account just one phenomenon

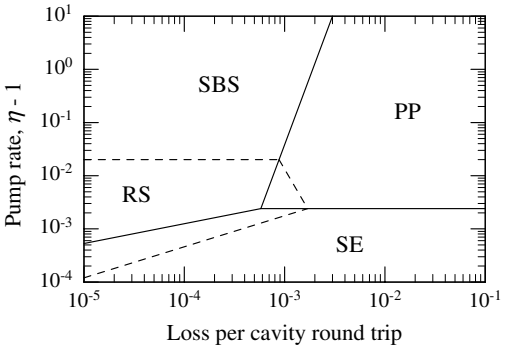

Fig. 12. Parameter regions of dominant limitations of sensitivity of a dye laser by spontaneous emission (SE), Rayleigh scattering (RS), stimulated Brillouin scattering (SBS), and population pulsations (PP)

at a time. The simultaneous action of PP and SBS may modify the position of the line of equal strength of PP and SBS in the diagram due to quenching of the beat notes of the light by PP. In contrast, SBS depends upon the beat notes $a^*_{p+q}a_p$, see last term of (40), but it does not react on them. The region where Rayleigh scattering is dominant represents the area of constant maximum sensitivity. It is enclosed by dashed lines that indicate an arbitrarily selected strength of Rayleigh scattering. If Rayleigh scattering is small enough, this area disappears and the highest sensitivity is reached at the merger point of the boundaries of the three areas SBS, PP, and SE.

The inclusion of dispersion into the model causes loss of sensitivity in the weak-dispersion regime, but growth at high enough dispersion. This anomaly complies well with the results of experiments [60]: the sensitivity has been shown to grow when the weak dispersion in the cavity owing to the presence of the gain medium and other optical elements is compensated by four prisms as compared to the laser without such compensation. Still further enhancement of the sensitivity, up to the fundamental sensitivity limit, is possible in a strongly dispersive cavity. However, the inclusion of additional dispersive elements in the cavity for sensitivity enhancement is again traded off by higher cavity loss that causes in turn some loss of sensitivity.

In solid-state lasers, four-wave mixing by the temporal part of PP is reduced in general by a much longer lifetime of the upper laser level. On the other hand, the active medium in a solid-state laser is usually longer than that of a dye laser, and four-wave mixing by the nonlinear electronic susceptibility must be taken into account.

Sensitivity quenching also results from the modulation of the pump laser by frequency components equal to the mode spacing of the laser [74, 75]. This modulation results from technical noise, or from self-mode-locking in the pump laser. In the latter case, corresponding modulation of the gain takes place. This modulation produces sidebands of the laser modes on the spectral positions of their neighbouring modes. Therefore, energy transfer takes place from the original modes to those neighbouring ones. The transfer rate varies as the photon number in the laser modes, and it can be formally treated in a similar way to Rayleigh scattering and be included in R of (37).

The identification of particular factors that limit the sensitivity in each type of laser allows one to optimize the laser

parameters for the most precise, sensitive, and reliable detection of ultra-weak or extremely rarefied absorbers.

6 Light fluctuations in laser modes

Except in the preceding Sect. 5.4, we have dealt with the dynamics of a multimode laser described in terms of *mean values* of the light flux in individual laser modes. Rate equation (7), for example, characterizes the mean values of photon numbers in the laser modes corresponding to experimental data averaged over many laser pulses, or over long integration time of cw operation. However, the weakness of mode coupling and the concomitant sensitivity to perturbation leaves this system susceptible to large variation of the light flux in individual laser modes. These fluctuations are described by (40), which takes into account stochastic excitation of the laser modes by spontaneous emission. In case of negligible mode coupling, $S = 0$, the trajectories of a mode signal exhibit full-scale quantum fluctuations [76, 77]. The autocorrelation time of these fluctuations, t_q, coincides with the spectral saturation time t_s if determined by spontaneous emission only; it is a few seconds according to (27). Under the influence of quantum fluctuations the laser is expected to show stochastic evolution [78].

The mean period of fluctuations observed with a dye laser is about 1 ms. Figure 13 shows photographically recorded spectrochronograms of the output of a cw multimode Rh6G laser at 0.5 GHz spectral resolution, for various values of the pump rate, η [79]. The spectrochronograms represent emission spectra of the laser, along the ordinate direction, which have been sequentially recorded, by a mechanical streak camera, in the abscissa direction. The length of the two-mirrors cavity was 15 cm, and the 1-GHz mode spacing is well resolved. The time resolution of these measurements is about 10 μs, and the horizontal lines represent individual laser modes. The emission in the laser modes indeed exhibits full-scale fluctuations. The autocorrelation time of these fluctuations, about 1 ms, is much shorter than that of quantum fluctuations, some 20 s, and it decreases as the pump rate increases, in contrast to quantum fluctuations, see (27). These short-time fluctuations result from nonlinear mode coupling that causes redistribution of the energy among the modes, with quantum fluctuations acting as the drive [63]. The time scale of the actual fluctuations is determined by the strength of mode coupling, i.e. by the last term on the right-hand side of (40). The short autocorrelation time of the fluctuations observed in the experiment corresponds to a short spectral saturation time, and to reduced sensitivity to ICA. This laser dynamics reveals the type and strength of mode coupling: dominating quantum fluctuations or mode coupling leave it stochastic or chaotic [80–82], respectively, the latter type of dynamics usually with a small number of effective degrees of freedom. Even regular dynamics is observed at very strong mode coupling [83].

The data of Fig. 13 demonstrate that the recording of a single laser spectrum at an arbitrary moment of time with high enough spectral resolution shows the absorption spectrum superimposed with enormous modal noise, such that the absorption is hardly identified. Averaging cancels the fluctuations, but not the absorption spectrum. As an example, Fig. 14 shows the emission spectra of n ($1 < n < 1024$) superimposed light pulses of a LiF:F_2^+ laser [84]. The pulse duration of this laser, 300 ns, is much shorter than the expected autocorrelation time of modal fluctuations. The cavity length is 25 mm, and the resolution of the spectrograph is just enough to resolve individual modes separated by 6 GHz. The single-pulse record ($n = 1$) shows large spectral fluctuations of the modal intensity, since the distribution of photon numbers in individ-

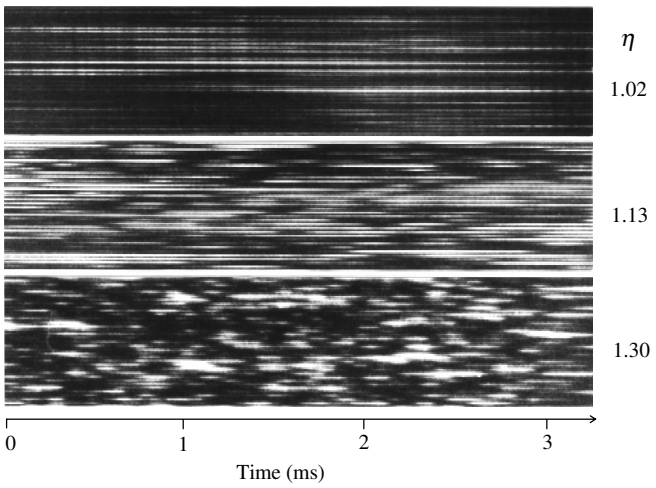

Fig. 13. Spectrochronograms of the output of a cw Rh6G laser at high spectral resolution, for various values of the pump rate, η. The *horizontal lines* are individual laser modes separated by 1 GHz [79]

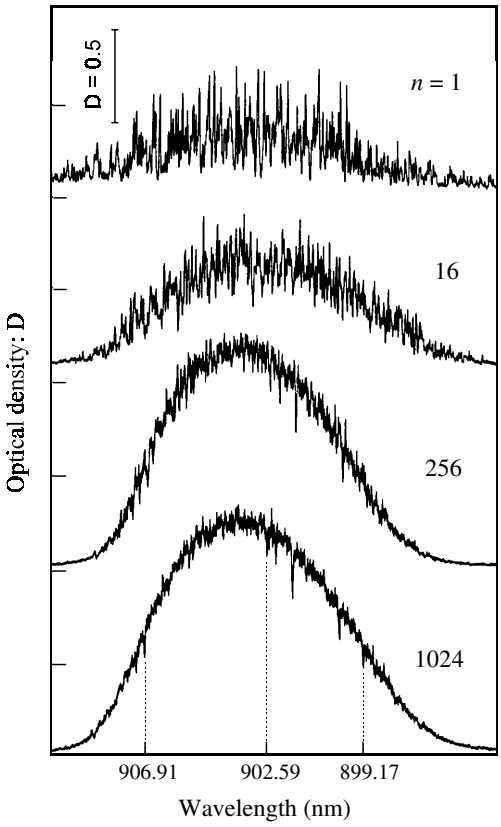

Fig. 14. Densitograms of photographically recorded spectra of n superimposed pulses of a colour centre laser. Cavity length $L = 25$ mm. Wavelength values of some ICA lines of water vapour are indicated [84]

ual modes obeys an exponential law [76]. The accumulation of light over many pulses reduces these fluctuations to such a low level that finally, at $n = 1024$, the intracavity absorption lines of atmospheric water appear. The deviations of the spectral flux from its mean value in multi-pulse spectra show a Gaussian distribution. The width of this distribution varies as in any random process, namely as the square root of the number of averaged laser pulses. At $n = 1024$, the amplitude of the spectral noise, $\Delta M_q \cong 0.03 M_q$, complies well with the last spectrum in Fig. 13.

Reduction of the spectral noise is achieved by integrating the signal over many laser *pulses*, as well as by integrating the signal over many laser *modes* or, in cw laser operation, by integrating the emission over a *time* interval much longer than the autocorrelation time of modal fluctuations. Thus, reduction of spectral noise is feasible by the increase of the number of oscillating laser modes upon extending the cavity length, if spectral resolution remains invariant. When measuring the absorption of water vapour at atmospheric pressure, the linewidth is about 5 GHz. With a 3-m laser cavity, 100 modes are averaged by the spectral recording of such a line by one laser pulse, and this recording would show 10% noise. Additional averaging, say, over 0.1 s at $t_s = 1$ ms, reduces the spectral noise to 1%. Averaging over transverse modes, if excited in the laser, would additionally quench the spectral noise.

7 Quantitative measurements by ICAS

Various strategies exist for quantitative measurements of ICA strength. We shall discuss here three most important variants: (i). Measurement of the absorption signals in the fourth time regime, i.e. under cw operation, when the laser emission spectrum is stationary. In this case, the calibration of the sensitivity to ICA is accomplished by recording the laser spectral dynamics and deriving the spectral saturation time t_s. Alternatively, the sensitivity may be calibrated by an ICA line whose absorption is known. (ii). Measurement of the absorption signals in the third time regime – i.e., under progressing spectral evolution – by means of a laser with well-defined pulse duration $t \ll t_s$. Here the absorption signal is determined by the time elapsed after the onset of laser oscillation, according to (23). (iii). Measuring ICA by a multimode laser with modulated gain.

7.1 Continuous recording

The first method of quantitative measurements under continuous laser operation, requires one to know the spectral saturation time. The absorption coefficient is then derived, according to (27), from the stationary absorption signal K_q^s:

$$\kappa_q = \frac{K_q^s}{ct_s} \,. \tag{43}$$

Although this type of measurements offers the highest sensitivity available with a particular laser, its accuracy suffers from the potential instability of the laser parameters: pump power, spectral position of the emission, laser threshold, cavity loss, etc. In particular, the spectral saturation time has to be controlled during the measurement, as may be done by recording the laser spectral dynamics, or by measuring the value of the absorption signal K_q^s corresponding to a calibrated absorption line in the laser cavity.

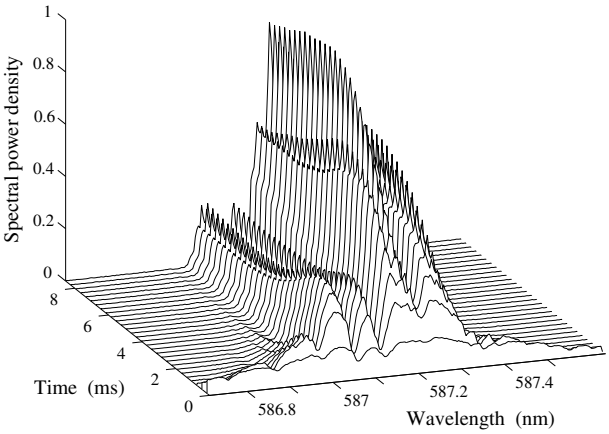

Fig. 15. Transient spectral dynamics of a Rh6G dye laser ($L = 68$ cm, $\gamma = 5.4 \times 10^6$ s^{-1}, $B = 2.6 \times 10^{-2}$ s^{-1}) with intracavity atmospheric absorption recorded at pump rate $\eta = 1.1$ [50]

The recording of the spectral dynamics of a Rh6G dye laser by ICA is demonstrated in Fig. 15 [50]. In this experiment, an argon pump laser is switched by means of an electro-optic modulator (EOM). Transient emission spectra of the dye laser are recorded with a spectrograph and a diode array by synchronizing the 0.3-ms-long reading cycles of the diode array and switching the laser. Every 32nd reading cycle of the diode array triggers the control signal of the EOM that stops the laser emission. The following reading cycle again triggers the EOM and starts the laser emission. As a result, the laser power is interrupted for one reading cycle of the diode array, and else is kept constant for a series of 31 subsequent reading cycles. The background noise signal accumulated by the diode array when shutting off the laser is subtracted from all the following 31 records. The signal obtained during the n-th reading cycle represents the emission spectrum of the laser at delay time t_n measured from the laser start up through the centre of the n-th reading cycle. The records have been averaged temporally over 128 series of cycles and spectrally over 9 longitudinal laser modes that contribute to the signal on each photodiode. Spectral noise is reduced to less than 3% by this averaging. Figure 15 shows, in a 3-D display a sampled set of spectra recorded at stepwise increasing the time delay t_n after the onset of laser oscillations. The spectral condensation of the laser output and the more and more increasing notches of the absorption dips that evolve according to (14) and (21) are recognized in the initial stage of laser dynamics. At the end of the recording, however, the spectral distribution is found stationary.

From the recorded dips the absorption signal is calculated using (22). The signal of the line at $\lambda = 587.224$ nm is shown in Fig. 16. Whereas the residual photon number $M_{q,\kappa}$ is represented by the signal in the centre of the absorption dip, the reference value M_q is obtained from the mean value of the signal of the diode array far enough on both wings of the absorption line. The data in the first phase of the evolution, at $t < 3$ ms, obey a linear fit, $K_q(t) = \kappa_q ct$ (23). This fit provides us with the value of the absorption coefficient in the centre of

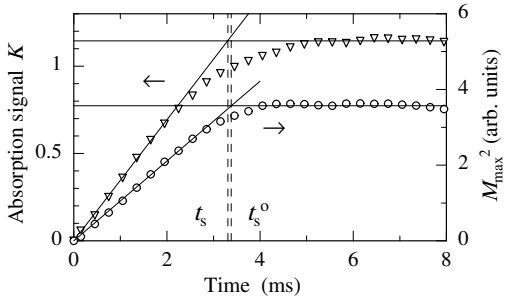

Fig. 16. (▽): Absorption signal K due to the water absorption line at $\lambda = 587.178$ nm in the output spectrum of the Rh6G dye laser, and (○): square of laser flux M^2_{max} in the maximum of the spectrum calculated from the data in Fig. 15, vs. the duration of the laser emission. t_s^0, t_s: spectral saturation times of emission and absorption, respectively

the measured absorption line, here $\kappa_q = 1.15 \times 10^{-8}\,\mathrm{cm}^{-1}$. At $t > 5$ ms the absorption signal saturates to the stationary value K_q^s. The crossing of the line $K_q(t) = K_q^s$ with the initial line of finite slope yields the spectral saturation time t_s. In this particular example, $t_s = 3.3$ ms. Note that varied parameters of the laser make the spectral saturation time vary within a wide margin, for example from 200 µs [24] to 230 ms [20].

The square of the light power in the centre of the emission spectrum is shown in Fig. 16 as well. As expected from (14) this quantity initially grows linearly with time. The spectral saturation time of emission t_s^0 required for reaching the stationary emission in the central mode is 3.4 ms. In this particular example it is just slightly higher than t_s, as it is with most dye lasers. However, in general the spectral saturation time of light emission t_s^0 may differ substantially from the corresponding time t_s of absorption, which is responsible for the sensitivity to ICA. It was shown above that with quantum-limited sensitivity $t_s^0 = t_s/\pi$ (see (18) and (27)). In a Ti:sapphire laser, for example, t_s^0 may far exceed t_s, see Sect. 9.3. Therefore, the derivation of the sensitivity to ICA from the measured saturation time of spectral narrowing of the laser *emission* is unreliable [31].

The spectral laser dynamics can be recorded also when a shutter in the output beam of the dye laser, for example, an acousto-optic modulator synchronized with the pump laser pulse, admits only a short pulsed fraction of the laser light to the diode array [38]. By varying the time delay of the gating pulse, this technique records data during the evolution of the spectra, from which all the relevant quantities are extracted. However, the procedure requires longer time to get results comparable with the above method, since parallel recording is replaced here by sequential recording. Photographic recording of the laser spectral dynamics is an alternative, for example, by combining the spectrograph with a mechanical streak camera [21, 79, 83].

7.2 Pulsed operation

The second method of quantitative absorption measurements is convenient when maximum sensitivity is not required. The recorded laser pulses of length τ extend inside the third regime of the spectral laser dynamics, and usually $\tau \ll t_s$. The spectral recording is done in one of two ways:

(i) The simplest procedure is time-integrated spectral recording of the laser emission by a photographic plate [85], a diode array [61, 86], or stepwise by a single photodetector [87]. The absorption signal is integrated over the total duration of the laser pulse and, for reduced noise, over many pulses. The value of the recorded absorption signal depends as much on the duration of the laser pulse as on the particular temporal evolution and spectral distribution of the laser output. If the spectral power density does not vary in time near the absorption line, the absorption coefficient is $\kappa_q = K_q/2ct$, as derived from integration of (23). In case of spectral condensation, according to (14), the absorption coefficient in the spectral maximum is $\kappa_q \cong 3K_q/5ct$ [61].

(ii) Another way is time-resolved spectral recording that involves the detection of the output spectrum over one short time interval Δt only, at the end of the laser pulse of length τ with $\Delta t \ll \tau < t_s$ [88, 89]. The absorption coefficient is derived according to (23) as $\kappa_q = K_q/ct$.

In this type of recording one has to be sure that the laser pulse duration is kept shorter than the spectral saturation time. Then, the sensitivity of measurements does not depend upon the position of the absorption line in the laser spectrum. Moreover, the results of these measurements depend neither on pump rate nor on cavity loss and are, therefore, not affected by any potential instability of laser power, or by air flow inside the cavity. However, the sensitivity to ICA is scaled down by τ/t_s.

7.3 Recording with a modulated pump

The third method of absorption measurements is the application of a multimode laser with its pump power modulated. The frequency of modulation has to be slightly lower than the intermode beat frequency, $\omega_0 = \pi c/L$ [74, 75]. Due to dispersion near the absorption line, mode spacings in the centre of the absorption line are increased, and in the wings decreased [90]. If the modulation frequency is tuned to resonance with particular mode spacings, the corresponding modes suffer smaller loss. As a result, the laser spectrum condenses into two emission lines on the wings of the absorption line. The spectral separation between these lines, $\Delta\omega$, varies upon scanning the modulation frequency or the cavity length. In the wings of the absorption line, where Lorentzian broadening dominates,

$$\Delta\omega = \sqrt{\frac{2c\beta L \int \kappa(\omega)\,\mathrm{d}\omega}{-\pi\,\Delta L}}\,, \tag{44}$$

with β being the filling factor, i.e. the fraction of the cavity filled with the absorber, and ΔL is the increment of the cavity length [75]. Resonance of the beat notes in these wings with the external modulation frequency requires the cavity length to be tuned shorter than the empty cavity. Measurements of the spectral separation $\Delta\omega$ of the line doublet at least at two values of the cavity length yield, according to (44), the spectrally integrated absorption coefficient $\int \kappa(\omega)\,\mathrm{d}\omega$, which is determined by the oscillator strength and the concentration of the sample. The accuracy of this type of measurement is very high. The spectral position of the doublet is independent of the stability of the effective absorption length L_{eff} and of the stability of other laser parameters. Pulsed lasers are applicable as well to this kind of measurement.

7.4 Nonlinear distortions of the line shapes of absorption

Sometimes particular nonlinearities appear with the recording of strong ICA lines. The nonlinear contributions to the signals are usually made observable by the dispersion associated with the absorption line. These nonlinearities belong to one of four categories:

The first one includes the condensation of the emission spectrum, i.e. the accumulation of spectral power near the absorption lines of resonant electronic transitions. The dispersion of the absorption line is responsible for the formation of an intracavity lens and for the corresponding modification of the stability range of the cavity in the wings of this line, if either the absorber distribution is spatially nonuniform [91], or the absorber is saturated [92]. A suitable remedy is shifting the operational parameters of the laser towards the centre of the laser's parameter range of stability.

The second category also displays some irregular spectral condensation close to the absorptive resonance. It is associated with the appearance of self-mode-locking by ICA, and with the dispersion near the absorption line [93–98]. The modulation of the light flux and laser gain is resonant with particular mode spacings somewhere at the absorption line. Other laser modes suffer extra loss, since their sidebands generated by the gain modulation, do not match the neighbouring modes, and decay. Indeed, modulation of the laser emission revealing mode-locking near ICA lines has been observed [97, 98]. This effect is restricted to strong resonant transitions, and reduced gas pressure, when the collisional broadening is smaller than inhomogeneous Doppler broadening. Complete modelling of this phenomenon would require the inclusion of the coherent interaction of both the absorber and the gain-providing molecules with the laser field in (40), a task that has not been performed yet. This distortion indeed affects the accuracy of absorption measurements, and self-mode-locking should be avoided.

The third category is characterized by an asymmetry of the ICA signal appearing as enhancement of the spectral flux at the high-frequency wing of the absorption line, and as reduction on the low-frequency wing [99, 100]. This modification of the absorption signal goes along with a corresponding asymmetry of the entire emission spectrum [62, 101]; it can be traced to the effects of SBS and/or PP [63, 73, 100]. The modification of the emission spectrum by SBS is caused by the antisymmetric spectral profile of the scattering function, and a corresponding Stokes shift of the laser emission [56, 63, 100]. The modification by PP is the result of the population pulsation's effect on the beat notes of the laser which results in a low-frequency modulation of the beat. Therefore, intermode beating takes place at a frequency that somewhat exceeds the frequency separation of the beating modes [63]. The dispersion in the cavity modifies the mode separation, and one group of modes can be brought into resonance with the modulation frequency of the polarization of the gain medium. This modulation, however, is determined by the beat notes of the majority of laser modes. The loss in this group of modes is reduced, and the intensity increases [51, 73]. The effect of PP is substantially reduced under diminished loss in the laser resonator, the effect of SBS by the application of a ring laser with unidirectional oscillation.

The fourth category shows enhanced background signals that are centred around the absorption lines and somewhat broader than these lines. A corresponding decrease of the background signal shows up with a gain line. This effect is caused by the spectral inhomogeneity of the gain, as it appears, for example by an insufficient relaxation rate of the lower laser level [100]. Since the light flux is spectrally constant within a particular homogeneous contribution to the gain profile, narrow-line intracavity absorption (or gain) is compensated by spectrally symmetric increase (or decrease) of the light flux within this homogeneous section of the profile [100, 102].

All these nonlinear distortions have been observed at high pump rate, usually with pulsed lasers. They turn insignificant or even disappear at lower light flux inside the laser cavity.

The identification of the physical origin of the observed nonlinearities in a particular experiment is prerequisite for the appropriate adjustment of the operational parameters of the laser in order to suppress undesired features in the spectrum. However, measurements under the majority of conditions have shown a linear response of the laser emission spectrum to ICA.

8 Combination of ICAS with noise-quenching signal recording

For complete characterization of the potential of an absorption measurement, the spectral sensitivity considered so far must be supplemented by a factor that indicates the quality of recording by the pertaining ratio of signal and noise. This "detectivity" is the inverse of the minimum detectable absorption signal, $K_{\min}$. High detectivity may considerably enhance the overall sensitivity when ICAS is supplemented with noise-reducing techniques of signal detection as, for example, in photoacoustic [46, 103], fluorescence [17, 104], optogalvanic [47], or saturation spectroscopy [62].

In conventional photoacoustic spectroscopy of gases for detection of weak absorption, laser light modulated by an optical chopper passes through a photoacoustic cell filled with the gaseous sample. Part of the absorbed radiation heats the gas and increases the gas pressure. Since the laser beam is modulated, the oscillating gas pressure generates an acoustic wave that is detected by a microphone and converted into an electric signal [4]. With a small signal, its strength is directly proportional to the laser power and to the absorption coefficient and, therefore, to the concentration of the sample in the PA cell. Spectral (and chemical) selectivity derives from scanning the frequency of the light source. Usually a narrow-band laser is used such that only at the resonances of the sample is an acoustic signal generated.

The application of a photoacoustic cell in ICA measurements requires some modifications of this technique. The sample cell with the trace gas to be measured is included in the cavity of a multimode laser. The laser should be switched off after a preselected lapse of time in order to set the required effective absorption path length, L_{eff}. Moreover, the output of the multimode laser is modulated, and the frequency of this modulation is made to equal the resonant frequency of the photoacoustic cell. Another photoacoustic cell placed in the output beam of the laser is filled with the trace gas at high concentration, such that one-way absorption in the cell is strong enough. The total pressures in the sample cell and detector cell should match each other, such that the absorp-

tion linewidths in both cells agree. Thus, the output light of the laser without ICA gives rise to a strong photoacoustic signal, if the laser light contains spectral components being absorbed in the sample. When, however, the intracavity cell is filled with the trace gas to be measured, light emission at the frequency components corresponding to the absorption decreases and reduces the photoacoustic signal. As a result, the absorption signal in this scheme is inverted: a weak photoacoustic signal corresponds to strong concentration of the trace gas in the sample. The dynamic range of this type of measurement may extend from 5 through 10 orders of magnitude [103]. It is determined by the signal-to-noise ratio of the ICA-less photoacoustic signal, by the stability of the emission spectrum of the laser, and by the jitter of the laser pulse length. The inherent averaging over a large number of ICA lines in the emission spectrum by the photoacoustic detection substantially increases the precision of this procedure.

In a different scheme for the enhancement of detectivity, the photoacoustic cell is placed directly in the cavity of a powerful single-mode laser [105]. In this case, some enhancement of the overall sensitivity is achieved not by better spectral sensitivity, but only because of the increased optical power inside the photoacoustic cell.

External fluorescence tubes and optogalvanic cells may likewise be used for enhanced detectivity in analogous schemes of detection [17, 47].

Moreover, ICAS may be supplemented in order to operate, in fact, as a variant of saturation spectroscopy [62]: the probe is placed in the cavity of the broadband laser, and the narrow-band radiation of a saturating laser is made to pump a well-defined transition in the probe. By the modulation of this narrow-band radiation, the population density in the initial and in the final state of the transition is made to vary with the frequency of the modulation. Within the emission spectrum of the broadband laser, all absorber transitions sharing a common level with the pumped transition will give rise to incremented or decremented spectral light power. This variation is revealed when using a phase-sensitive detection technique, for example a monochromator combined with lock-in amplifier. Signals from other transitions, whose energy levels are populated by energy transfer from the pumped level, will also show up, but with a phase difference, determined by the rate of energy transfer. The maximum signal is achieved when the modulation frequency is smaller than or equal to $1/t_s$. Note that such a measurement provides Doppler-free absorption spectra, whose resolution is limited by the bandwidth of the narrow-band laser. Moreover, the sensitivity of detection of the absorption signal is increased, since it is not measured on the background of the strong fluctuating emission spectrum, but on zero background. The fluctuations of the laser modes outside ICA lines do not contribute to the output signal. This scheme is also applicable with narrow-band saturation of another line that shares a common level with the absorber line ("cross-saturation" spectroscopy).

9 Sensitive ICA measurements with various types of lasers

Most available types of multimode lasers, emitting both cw or long enough pulses, have been applied to the detection of ICA, although their specific dynamics makes vast differences of sensitivity prevail. In order to appreciate the respective usefulness of a particular laser for the detection of gaseous traces, inspection of two quantities suffices: the effective absorption path length, which characterizes the sensitivity of the measurement, and the bandwidth of the emission spectrum which characterizes the amount of spectral information simultaneously obtained with a single measurement. In this section we review these quantities as obtained from the dynamics of various types of lasers. Table 1 shows the highest sensitivity, corresponding spectral saturation time, the origin of sensitivity limitation, and the bandwidth of spectral emission, that have been achieved with these lasers.

Table 1. The values of spectral saturation time t_s of absorption, effective absorption path length L_{eff} and the emission bandwidth $\Delta\nu_{exp}$ (HWHM) achieved in ICAS measurements with various lasers. The origin of the limitation of sensitivity is indicated as FWM for four-wave mixing, RS for Rayleigh scattering, SE for spontaneous emission, and τ for limitation by the laser pulse duration

Laser type	t_s /ms	L_{eff} /km	Limitation	$\Delta\nu_{exp}$ /GHz
Dye [20]	230	70 000	FWM	45
Ti:sapphire [112]	4.5	1300	FWM, RS	100
Diode [52]	0.13	40	SE	3
Fibre [54]	0.43	130	RS	1500
Nd^{3+}-glass [110]	12	3600	τ	300
CCL [117]	0.4	120	τ	3000
OPO [123]	5×10^{-6}	0.0015	τ	200

9.1 Nd^{3+}*-doped glass laser*

An early broadband laser applied to ICAS was the flash-lamp-pumped Nd^{3+}-doped glass laser [14, 15]. Already the first measurements have demonstrated the effective absorption path length $L_{eff} \cong 300$ km, set by the 1-ms duration of the laser pulse. The inhomogeneous broadening of the gain line as a consequence of the distribution of the Nd^{3+} ions over non-equivalent sites in glass allowed spectrally broad emission, from 1.055 to 1.067 μm, recorded in each pulse of the laser. Weak absorption spectra of many molecular species, such as CO_2, CH_4, C_2H_2, C_2HD, NH_3 [106], and H_2O, HN_3, HCN [107], have been recorded in this spectral range for the first time.

The spectral dynamics of Nd^{3+}-doped glass lasers differs from that of dye lasers commonly used with ICAS in two respects:

(i) It is a "class B" laser [108] (as most other solid-state lasers) where the resonator loss rate γ exceeds the rate of spontaneous emission, $\gamma > A$. Laser inversion does not adiabatically follow the photon number in the laser cavity, as in dye lasers, and damped relaxation oscillations take place in the transient regime of laser dynamics. But as long as the power in individual laser modes does not drop below the level of spontaneous emission – which is so under most real conditions – these oscillations do not perturb the evolution of the absorption signal, and the modified Lambert–Beer law of (21) holds. Measurements of the spectral dynamics of a Nd^{3+}-doped glass laser [21, 109] have confirmed the validity of (21).

(ii) Spectral condensation does not take place in this laser since the gain is inhomogeneously broadened. The total emis-

sion spectrum does not narrow as it does with lasers running on homogeneously broadened gain, but, in contrast, widens with the duration of laser oscillation [21, 108] owing to the delayed excitation of ions whose resonances are somewhat shifted off their vacuum frequency. The condition for highly sensitive multimode ICA measurements holds for each individual class of ions, since the homogeneous linewidth exceeds the width of absorption lines. Increasing the laser pulse duration up to 12 ms has demonstrated the expected growth of sensitivity, and the maximum value approached $L_{\mathrm{eff}} = 3600$ km [110]. No competing limitation of sensitivity has been recognized so far: Further enhancement of the sensitivity may be feasible by increasing the pulse duration, but was actually hampered by the thermal distortion of the active medium.

The spectral range covered with this type of laser has been extended to 1.050–1.083 μm when using a Brewster prism inside the cavity [111].

9.2 Dye lasers

Multimode dye lasers have been widely used with ICAS so far. They operate in the visible and near IR and can be pumped by a pulsed laser, by a flash-lamp, or by a cw noble-gas laser. Exceedingly high sensitivity to ICA has been shown achievable with cw dye lasers [20, 60, 61]. The sensitivity in these lasers is ultimately limited by the nonlinear interaction of light and gain medium, namely by four-wave mixing due to population pulsations [63, 73]. This nonlinearity varies as the cavity loss (42), and as the overlap integral of the modes in the gain medium which contributes to the coefficient R of (40). Although in unidirectional ring lasers the overlap of laser modes in the gain medium is smaller, the cavity loss usually exceeds that of standing-wave lasers. Therefore the sensitivity in both these laser types assumes about the same level. However, interference of the laser light with light reflected or scattered from all the optical components is smaller in the cavity of a unidirectional ring laser, and the spectrum of this laser is less sensitive to such spectral distortions and has less spectral noise [37].

Figure 17 shows an example of the spectral dynamics of a Rh6G dye laser with high sensitivity. The data have been recorded by a spectrograph and a diode array, as in Fig. 15. The laser parameters of this experiment are $L = 3$ m, $\eta = 1.01$, $\gamma = 10^6\ \mathrm{s}^{-1}$, $B = 6 \times 10^{-3}\ \mathrm{s}^{-1}$, and $Q = 7.5 \times 10^5$. The loss, 2% per cavity round trip, is identified as intrinsic cavity loss, such as absorption in the dye, and scattering and absorption in the mirrors; it cannot be reduced any more. The evaluation of the fundamentally limited spectral saturation time by (28) yields 7 s for small absorption lines near the emission maximum.

The absorption signal K of three lines, $\lambda_1 = 586.941$, $\lambda_2 = 587.000$, and $\lambda_3 = 587.013$ nm, is shown in Fig. 18 (top) depending upon the duration of laser emission. The absorption coefficients of these lines, obtained from the corresponding initial slopes of $K(t)$, are 1.24×10^{-9}, 1.51×10^{-9}, and $5.01 \times 10^{-10}\ \mathrm{cm}^{-1}$, respectively. The absorption signal of the line $\lambda_1 = 586.941$ is obtained by averaging over only 8 records of the spectral dynamics and is, therefore, noisier than the other two absorption signals averaged over 80 records. The mean value of the spectral saturation time determined from these absorption signals is $\langle t_{\mathrm{s}} \rangle = 70\ \mathrm{ms} \pm 3\%$. The absorption lines are rather strong, and the laser power in the stationary spectrum in the centre of the absorption lines drops down to 0.05–0.3. From (30) and (27) one derives the fundamentally limited spectral saturation time to be somewhere in the range 0.35–2 s, which is larger than the recorded value, 70 ms. This finding indicates that the sensitivity of the dye laser to ICA is not primarily affected by spontaneous emission, but by other effects such as nonlinear mode coupling and/or Rayleigh scattering.

Figure 18 (bottom) shows the square of laser flux at the maximum of the spectral envelope, M^2_{max}, at $\lambda = 587.004$, calculated from the data in Fig. 17, vs. the duration of laser emission. This dependence provides us with the spectral saturation time of emission, $t_{\mathrm{s}}^0 = 108$ ms, which is 50% larger than t_{s}. The discrepancy between t_{s}^0 and t_{s} has been traced to

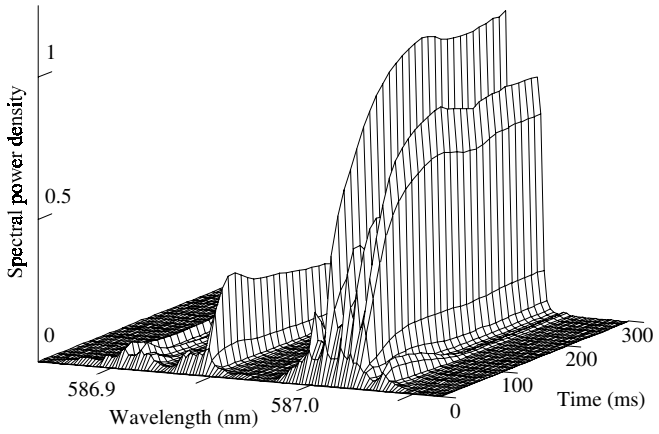

Fig. 17. Transient spectral dynamics of a Rh6G dye laser ($L = 3$ m, $\gamma = 10^6\ \mathrm{s}^{-1}$, $B = 6 \times 10^{-3}\ \mathrm{s}^{-1}$) with intracavity atmospheric absorption recorded at pump rate $\eta = 1.01$

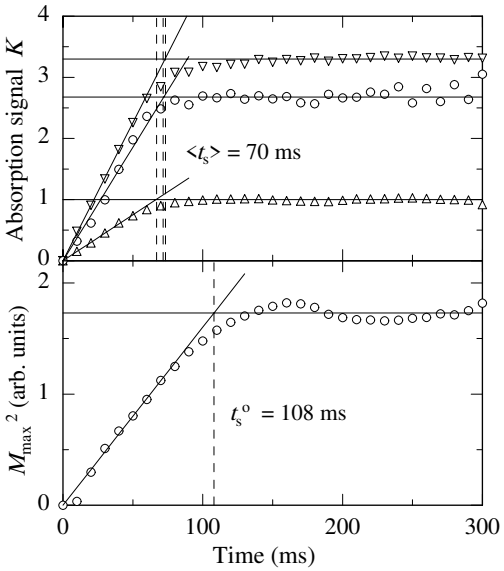

Fig. 18. Absorption signals K of atmospheric absorption lines at 586.941 nm (○), 587.000 nm (▽), and 587.013 nm (△) (*top*), and square of laser flux M^2_{max} in the maximum of the spectrum (*bottom*) calculated from the data in Fig. 17, vs. the duration of the laser emission. $t_{\mathrm{s}}^0, t_{\mathrm{s}}$: spectral saturation times of emission and absorption, respectively

the effects of four-wave mixing and dispersion on the laser spectral dynamics [73]. These effects limit the sensitivity to ICA and produce additional loss for weak modes. Therefore the value of t_s^0 cannot be used as a measure for sensitivity replacing t_s as has been suggested [31, 60].

In order to visualize the sensitivity of ICA measurements, we estimate the absorption signal of Na atoms ($3S_{1/2} \rightarrow 3P_{3/2}$) at the concentration $n = 1\,\mathrm{cm}^{-3}$ in the cavity of a cw Rh6G laser with the so far highest available sensitivity, $L_{\mathrm{eff}} = 70\,000\,\mathrm{km}$ ($t_s = 230\,\mathrm{ms}$) [20]. For a naturally broadened transition ($\delta\nu = 10\,\mathrm{MHz}$), for example in an atomic beam intersecting the cavity, the absorption coefficient in the line centre of absorption is $\kappa = n\sigma = 1.1 \times 10^{-9}\,\mathrm{cm}^{-1}$. This loss generates a strong signal of absorption, $K = 7.7$, in the emission spectrum, corresponding to 2000-fold reduction of the spectral power density at the line centre. If the Na atoms are confined in an absorption cell, their resonance line is Doppler-broadened ($\delta\nu = 1.3\,\mathrm{GHz}$), and $\kappa = 1.2 \times 10^{-11}\,\mathrm{cm}^{-1}$. The reduction of the spectral power density at the line centre is 9% ($K \cong 0.09$) in this case, which still suffices for detecting with good signal-to-noise ratio. These examples demonstrate the potential of ICAS for spectroscopy of individual atoms or even molecules.

9.3 Ti:*sapphire laser*

A titanium-doped crystal displays gain that extends from 670 nm to 1.1 μm. This kind of crystal meets rather well the requirements for sensitive ICAS. However, its application to ICAS is restrained by the intrinsic birefringence of the sapphire which in general causes spectral modulation of the output. In order to avoid this complication, the C axis of the crystal has to be set parallel to the optical axis of the laser cavity, or perpendicular to both the axis of the cavity and the electric field vector of the laser emission. In the latter case the laser gain is higher than in the former one, and only the ordinary beam is generated [30]. The sensitivity of this laser type to ICA ranges from 50 km [29] to 1300 km effective absorption length [31, 112], depending on the laser parameters. This sensitivity is much smaller than what is expected from the limiting effect of spontaneous emission. According to (29), the fundamental sensitivity limit is 3×10^8 km ($t_s = 1000\,\mathrm{s}$), calculated with laser parameters taken from experiment [112] ($A = 3 \times 10^5\,\mathrm{s}^{-1}$, $B = 1 \times 10^{-6}\,\mathrm{s}^{-1}$, $Q = 6 \times 10^5$, $\gamma = 3 \times 10^6\,\mathrm{cm}^{-1}$, $L = 2\,\mathrm{m}$, at $\eta = 1.3$).

The sensitivity to ICA of a cw Ti:sapphire laser does not depend much on the pump power; in fact it decreases very weakly upon increasing pump power [29–31, 112]. From this observation one concludes that Rayleigh scattering is the dominant perturbation of the spectral evolution and limits the sensitivity, in contrast to a dye laser, whereas the effect of nonlinear mode coupling is secondary in the crystal. Four-wave mixing by PP in a Ti:sapphire laser is almost absent, since the rate of population decay of the upper laser level is about 10^3 times smaller than in the dye laser. In this situation, nonlinear mode coupling by four-wave mixing due to other nonlinearities in the crystal, for example of electronic type, dominate the influence of PP. Indeed, a degenerate version of electronic nonlinearity, the Kerr effect, is relatively strong in Ti:sapphire crystals and responsible, for example, for the observed self-mode-locking of this laser [113]. Thus,

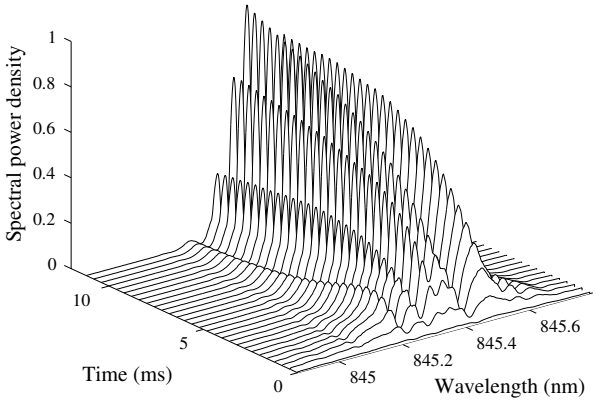

Fig. 19. Observed transient spectral dynamics of a Ti:sapphire laser with intracavity water absorption

it is natural to assume that this particular type of four-wave mixing contributes to the spectral dynamics in this crystal laser, further reduces the laser's sensitivity to ICA, and produces additional loss at weak modes, similar to the effect of PP in dye lasers.

Figure 19 shows a temporal sequence of emission spectra obtained with a Ti:sapphire laser [112] and recorded with a spectrograph and a diode array, like the data of Fig. 15. The Ti:sapphire laser operated in a linear standing-wave configuration whose parameters were set as above. The absorption signal at $\lambda = 845.352\,\mathrm{nm}$, and the square of the light flux at the maximum of the spectral envelope, M^2_{max}, at $\lambda = 845.37\,\mathrm{nm}$, versus the duration of laser emission, are shown in Fig. 20a. The absorption coefficient κ_q of this line, calculated from the linear fit $K_q = \kappa_q ct$, is $1.03 \times 10^{-8}\,\mathrm{cm}^{-1}$. The absorption signal saturates after $t_s = 3.8\,\mathrm{ms}$ to its stationary value. In contrast, the square of the laser flux in the peak of the spectrum does not show any saturation at this time. Figure 20b shows again the square of the light flux at the emission peak versus the duration of laser emission, but on

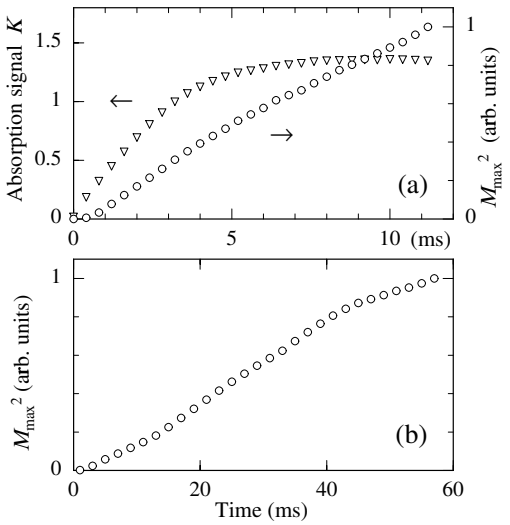

Fig. 20a,b. (▽): Absorption signal K of water absorption line at 845.352 nm, and (○): square of laser flux M^2_{max} in the peak of the spectrum, calculated from the experimental data in Fig. 19 (**a**), and from the data with five times extended duration of reading cycles (**b**), vs. the duration of laser emission

a compressed time scale. The data just hint to beginning saturation, and the saturation time t_s^0 of spectral evolution of the peak emission much exceeds that of the absorption signal and the 60-ms maximum recording time, in contrast with the relationship $t_s = \pi t_s^0$ of Sect. 4.

The two saturation times t_s^0 and t_s seem to differ for the mode coupling by four-wave mixing caused by the nonlinearity of the host material, and for the dispersion in the cavity. The beat notes of the laser modes in the centre of the emission spectrum modulate the electronic polarization in the host material. Dispersion leaves this modulation off-resonant with the spacings of the modes in the rest of the spectrum. Therefore, light scattered from each of these modes decays and does not contribute to any neighbouring mode. As a result, weaker modes acquire extra loss. In this case, condensation of the laser spectrum to the stationary state results from *both* the gain profile of excited ions as in (18), *and* the nonlinear extra loss. This additional contribution to the loss grows with the light flux, and will modify the spectral variation of the net gain. When the gain varies more than expected from (9), the condensation advances faster than indicated by (15). This situation is shown in Fig. 20b, where the slope of $M_q^2(t)$ increases even at $t > 10$ ms. This process saturates when the number of oscillating modes has declined.

Such a scenario of accelerated condensation of the emission spectrum of a Ti:sapphire laser at $t > 10$ ms, with t_s being only 3 ms, has been also recorded in earlier experiment with a Ti:sapphire ring laser at $\eta = 1.8$ [31, Fig. 5]. Furthermore, modulation of the laser output at the beat frequency of the modes has been observed. The degree of this modulation increases as the laser pulse duration grows [31, Fig. 8]. These observations support the above assumption. With that actual type of nonlinearity, the sensitivity limits of linear and ring lasers agree.

The spectral width of laser emission at t = 4 ms was found to be 100 GHz (HWHM) [112], which is assumed to be the spectral width of laser oscillation narrowed by a Brewster prism used for wavelength selection, and by intracavity absorption. The output spectrum of the ideal laser is expected to be 560 GHz wide, according to (15).

The results of Fig. 20 indicate that the dynamics of the absorption signals should not be identified with the dynamics of spectral condensation which feigns too high sensitivity of ICAS in the Ti:sapphire laser. The data show that the spectral saturation time of emission is at least 20 times that of the absorption signal. Previously, the value 120 ms has been found as the spectral saturation time of emission, 40 times longer than that of the absorption signal (3 ms) [31]. Thus we emphasize that only the spectral saturation time of *absorption*, t_s, yields a reliable effective absorption path length.

9.4 Colour centre lasers

Colour centre lasers (CCL) for ICAS operate in the spectral range 0.6 μm through 3 μm [114], where the fundamental vibrational bands of most molecules are located, and ICAS promises both high sensitivity for the detection of low concentration, and high selectivity for the discrimination of molecular species. However, most cw CCL require cooling by liquid nitrogen, and their spectrum condenses into very few modes only [115] due to the small spectral width of the gain. Thus, ICA measurements seem restricted to pulsed-laser operation [43]. CCL convenient for use in ICAS measurements are LiF:F_2^+ [26, 27] and LiF:F_2^- [28, 116] lasers that operate at room temperature and in broad spectral ranges in the near IR. Measurements of the absorption of H_2O, HDO, and CH_4 with LiF:F_2^- lasers have been reported in the range 1.1 μm through 1.25 μm. The maximum sensitivity achieved corresponds to $L_{\text{eff}} = 60$ km [116] and was set by the $t = 200$ μs laser pulse duration. Measurements of ICA with LiF:F_2^+ are possible in the range 890–970 with $L_{\text{eff}} \cong 100$ km [117]. Some other types of CCL have been proved suitable for ICAS measurements, for example a NaF:F_2^+:F_3^- laser in the range 0.98–1.4 μm [118], a NaCl:F_2^+ laser in the range 1.48–1.56 μm [44], and a KCl:Li F_a (II) laser in the range 2.6–2.7 μm [43].

9.5 Diode lasers

Although the performance of certain lasers in ICAS applications seems promising, their practical application may be prohibitive nonetheless for their delicate, bulky, or expensive set-up. From this viewpoint diode lasers seem attractive. Unfortunately, their performance is inadequate on various counts: (i) The gain width in diode lasers is rather small, and only a very narrow spectral interval can be investigated with one laser pulse. (ii) Commercial diode lasers have to be specially prepared for their application with ICAS, and they must be equipped with an external cavity. One or both [32] of their facets must become antireflection-coated, or they should be cut at Brewster's angle to the optical axis [33] in order to minimize periodic structures in the output spectrum generated by parasitic internal etalons and named "spectral channelling". (iii) Diode lasers show loss in the diode channel that may be as high as 70% per single path [32], and therefore their sensitivity is curtailed even by spontaneous emission. With the typical laser parameters $A = 10^9\ \text{s}^{-1}$, $B = 10\ \text{s}^{-1}$, and $\gamma = 10^9\ \text{s}^{-1}$ [32], and with the pump rate $\eta = 1.1$, the fundamental limit of sensitivity is only $L_{\text{eff}} = 2.5$ km.

All the measurements reported so far have been performed by GaAlAs lasers at 770 nm [33], and at 780 nm wavelength [32, 52]. A linear diode laser with one AR-coated facet shows strong spectral channelling, and at 1% above threshold already operates in one of these channels only [32]. A ring resonator with both facets AR-coated is less susceptible to spectral modulation since two reflections from AR-coated facets are required to build up an interference pattern [52]. The sensitivity of detection grows with the pump power up to 4% above threshold (see Fig. 9). At higher pump rates, other perturbations of coherence seem to appear and dominate the laser dynamics. The highest sensitivity obtained so far with diode lasers corresponds to $L_{\text{eff}} = 40$ km, with the emission bandwidth being just 3 GHz (HWHM). At this level of sensitivity, even one pair of planes with low reflection in the ring cavity produces strong spectral modulation. This modulation can be reduced, however, by cutting a diode facet at Brewster's angle [33].

The technological progress in manufacturing and preparation of diode lasers will presumably improve their sensitivity and future applicability for ICAS in the extremely useful accessible spectral range 0.4 μm through 30 μm.

9.6 *Doped fibre lasers*

Doped fibre lasers are actually doped glass lasers, as described in Sect. 9.1, but manufactured as waveguides for the pump and laser light. Fibre lasers operate continuously on numerous ionic transitions of various rare earth dopants, such as Nd, Yb, Pr, Tm, Er, Ho, in the range of 0.45 through 3.9 μm [119]. The high concentration of the pump and laser light in a small channel (usually 2–5 μm wide) allows efficient transfer of the pump power to the active ions and ensures high gain. As a result, fibre lasers operate upon diode-laser pumping with their typical pump threshold below 1 mW. The combination of laser and pump laser can be manufactured as a compact unit that consumes low power in accordance with the requirements of field measurements of IC absorption [34]. Important advantages of fibre lasers over diode lasers are their low loss and the inhomogeneous broadening of their gain which allows for measurements of ICA in a broad spectral range with no spectral tuning. The internal loss in the fibre is in fact negligibly small, and the overall cavity loss may be as low as 10% per round trip which results mostly from the poor efficiency of the optical coupling of the external part of the cavity to the fibre. Measurements of relaxation oscillations of the laser output after incrementing the pump power allow for the determination of the cavity loss and of other parameters, including the nonlinearities of the gain-providing glass [120].

The sensitivity of a Nd^{3+}-doped fibre laser to ICA does not depend on the pump excess in the broad range $0.1 < \eta - 1 < 10$ (see Fig. 9), and it is limited to its asymptotic value probably by Rayleigh scattering in the fibre [53, 54]. The effect of Rayleigh scattering is here stronger than in a bulk glass laser, since the divergence of the light in the fibre is larger, and so is the acceptance angle for Rayleigh scattering being coupled into the laser mode [59]. The highest sensitivity of ICA measured by a Nd^{3+}-doped fibre laser has been found to yield $L_{\mathrm{eff}} = 130\,\mathrm{km}$ [54]. The bandwidth of stationary emission is as high as $1.5 \times 10^3\,\mathrm{GHz}$ (HWHM) at $\eta \cong 10$. The emission spectrum is easily tunable within a broad range with some selective element such as a prism or a dispersive lens inside the cavity. Figure 21 shows an example of superimposed emission spectra of a Nd^{3+}-doped fibre laser obtained by tuning the emission spectrum by a dispersive lens [54]. With the use of a single set of cavity mirrors, the spectrum extends over two transition bands in the Nd^{3+} ion, $^4F_{3/2} \rightarrow {}^4I_{9/2}$ (0.9–0.945 μm) and $^4F_{3/2} \rightarrow {}^4I_{11/2}$ (1.075–1.145 μm). This tuning feature allows for measurements of absorption of a great variety of molecular species by the same experimental arrangement.

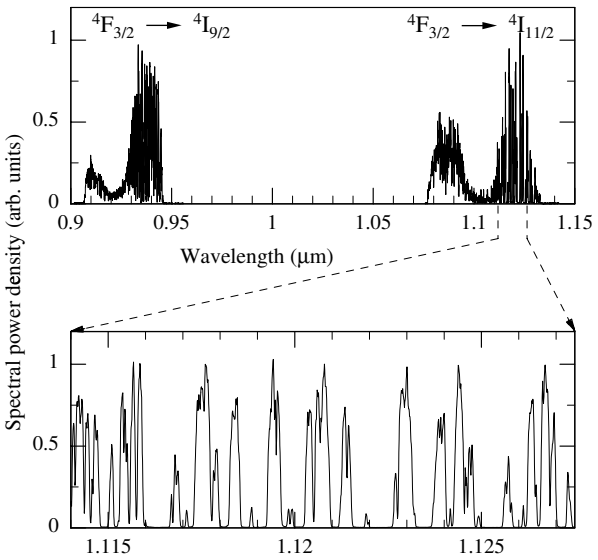

Fig. 21. Output spectrum of a Nd^{3+}-doped fibre laser with intracavity atmospheric absorption

9.7 *Other solid-state lasers*

Many other solid-state lasers are also applicable for ICAS measurements. In spite of its relatively narrow gain profile, a ruby laser has been used for measurements of the absorption spectrum of water vapour at 694 nm [121]. The 0.6-cm^{-1}-wide emission spectrum had been tuned over 6 cm^{-1} by varying the temperature of the ruby crystal. Better opportunities for wide-band spectral recording offer laser crystals with a broad gain spectrum, for example Cr^{3+}:YAG operating in the range 1.38–1.55 μm [42], or Co:MgF_2 operating in the range 1.6–2.5 μm [45].

9.8 *Optical parametric oscillators*

Multimode optical parametric oscillators (OPO) have been also suggested for use with ICAS [122]. Their signal and idler light waves, at frequencies ω_s and ω_i, are generated by light of a narrow-line pump laser at the frequency ω_p with the help of a nonlinear crystal, for example, BBO. The degree to which the three wave-vectors obey the phase-matching condition $\omega_p = \omega_s + \omega_i$ defines the spectral bandwidth of both the signal and idler light. If the cavity includes ICA and therefore some modes of, say, the idler wave decay quickly, signal light also decays at the corresponding frequencies. The potential of ICAS with OPO includes: (i) broad tuning range of the multimode laser emission from a single pump source, and (ii) measuring ICA of the IR idler light by recording the signal light in the *visible* emission spectrum leaving the spectral recording much easier. The drawback of this use of an OPO is the rather narrow emission spectrum owing to the intrinsic resonant conditions.

In the only experiment performed so far on ICAS by an OPO the absorption of acetylene at 1.53 μm in the cavity of the idler wave has been measured in the spectrum of the signal wave at 461 nm [123]. The duration of the laser pulses was only 5 ns, and the effective absorption path length did not exceed $L_{\mathrm{eff}} = 1.5$ m. The spectral width of converted IR emission, 200 GHz (HWHM), was increased by using divergent pump light. However, the operation of the idler wave would turn single-mode already after 100 μs of laser action, which imposes the narrow limit on the sensitivity of ICAS with this particular OPO.

10 Applications of ICAS

ICAS is distinguished by specific beneficial features: (i) high sensitivity, (ii) parallel multichannel spectral recording, (iii) high time resolution, and (iv) no interference by background

light from the sample. High sensitivity allows one to measure spectra of very weak absorption or gain, caused either by a small number of molecules, or by weak transitions. Numerous absorption lines of one or more species can be recorded simultaneously in one pulse of laser emission, impossible with any other laser technique of sensitive detection. Time resolution can be as good as a few ns, although the required sensitivity may necessitate longer unimpeded oscillation, i.e. lower temporal resolution. Light-emitting absorptive samples, as they occur, for example, in studies of combustion, explosion, etc., neither generate a background nor any additional noise to the signal. ICAS is the only technique adapted to the investigation of processes that go on under all these complicating conditions: for example, when recording the transient kinetics of chemical reactions in multicomponent gas mixtures. We account here for certain principal examples of ICA measurements that have been successfully applied to the solution of a wealth of various problems.

10.1 Measurements of weak line absorption

10.1.1 Atmospheric extinction. Even the first recordings of output spectra of lasers whose cavities contained air have demonstrated many unknown absorption lines [107, 124, 125], when compared with spectra of solar absorption [126]. The sunlight's absorption path length in the atmosphere does not exceed some tens of km, whereas the effective absorption path length in the above ICAS experiments is some hundreds of km. Furthermore, many atmospheric absorption lines could not be detected in the spectrum of solar absorption, since they are superimposed with absorption in the solar corona.

The most complete information on the absorption of many atmospheric compounds is accumulated in the HITRAN database [127]. Figure 22 shows, as an example, a section of atmospheric absorption obtained in the cavity of a multimode Rh6G dye laser, and the corresponding section calculated from the HITRAN database [128]. The effective absorption path length of ICA has been $L_{\text{eff}} = 330$ km, set by detecting for 0.17 ms, starting 1.02 ms after the onset of laser oscillation, with an experimental set-up similar to the one described in Sect. 7. The laser emission was recorded by a spectrograph and a diode array at a combined spectral resolution of 2.4 GHz ($0.08\,\text{cm}^{-1}$). The mode separation frequency is 64 MHz. Each spectral record is averaged over 2048 laser pulses. Averaging over many laser pulses as well as over many modes within the interval of spectral resolution reduces to 0.4% the noise that results from mode fluctuations. The entire absorption spectrum in the range from 571.3 nm to 604.3 nm has been composed from individual overlapping emission spectra of 0.3-nm bandwidth each. The observed spectrum consists mostly of overtones of atmospheric water absorption. It is juxtaposed with an atmospheric spectrum calculated from the HITRAN database with the absorptive path length set to 330 km, and the temperature 296 K, convolved with the apparatus function of the spectrograph. Only water vapour at the concentration of 7.39×10^{-3} is found to absorb light, according to the database. The spectral positions and the strengths of most of 581 water vapour lines contained in the database are well reproduced by the observed spectrum. However, 10 lines are found missing in the ICA spectrum, shifted in frequency by more than 10 GHz, or having a different line strength (at least by a factor 2). In addition, the ICA spectrum contains 104 new lines whose absorption signal is at least $K_{\min} = 0.12$, which definitely exceeds the spectral noise of the record and corresponds to the absorption coefficient of $3.8 \times 10^{-9}\,\text{cm}^{-1}$. Some of the novel absorption lines are indicated in Fig. 22 by arrows. This observation proves the feasibility of accurate quantitative measurements of both spectral positions and strengths of weak absorption lines by ICAS.

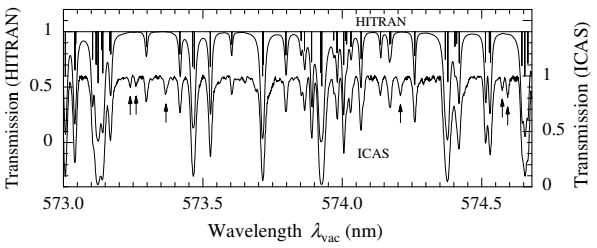

Fig. 22. Section of the atmospheric transmission spectrum synthesized from HITRAN data (*upper record*), and ICA spectrum obtained with Rh6G laser at $L_{\text{eff}} = 330$ km (*lower record*) [128]; *vertical lines* in the *upper record* represent the HITRAN data of spectral position and relative strength of absorption lines in a logarithmic scale ($\times 10$ corresponds to 1/4 on the ordinate scales). *Arrows* indicate new absorption lines found by the ICA measurements

10.1.2 Molecular spectroscopy. A considerable wealth of spectral data on various molecular species has been collected in those spectral intervals accessible by lasers. Molecular overtone absorption in the visible and near-IR spectral ranges is, as a rule, very weak and can be hardly detected by conventional measurements of absorption. The high sensitivity of ICAS permits one to investigate quantitatively various features of these weak absorption spectra of numerous molecules. Spectroscopic studies of the molecules require, sometimes, only measurements of the spectral positions of absorption lines. In these cases the exact determination of the sensitivity is unimportant, and the measurements can be carried out with a cw laser disregarding the achieved spectral sensitivity as long as the spectral signal is strong enough.

In the visible range, ICAS usually makes use of dye lasers. Highly forbidden transitions of O_2, for example, have been recorded around 630 nm [129] with rhodamine B, or around 580 nm [130] with rhodamine 101 and 110 dye lasers. In the range near 630 nm, the absorption strength and collisional broadening of individual rotational lines of O_2 have been measured in detail [88, 131]. The overtone spectra of heteronuclear molecules have been studied in the visible as well [132]: rotational constants of the sixth harmonics of transitions of $H^{35}Cl$ and $H^{37}Cl$ were recorded in the spectral range about 635 nm [129]. The rotational structure of CHD_3, CHF_3 [133], SiH_4 [134], $SiHD_3$ [132], CH_4, NH_3 [135], GeH_4 [136], N_2O [137], H_2S [138], HOCl [139], and C_2D_2 [140] has been analysed in detail in the spectral range from 500 nm to 1 μm by means of various dye lasers, or with a Ti:sapphire laser. Vibrational spectra of ICA of O_3 with their spectral resolution as good as 0.42 GHz have revealed radiative line broadening by predissociation and yielded estimates of the lifetimes of the lowest excited (triplet) state [141]. Absolute values of absorption coefficients of CO_2 overtone lines have been derived from time-

resolved recordings of the emission spectrum of a Ti:sapphire laser with ICA [142].

The absorption spectra even of small molecules are usually rather complex. Their identification may be simplified by the suppression of hot-band absorption at low temperature. Expansion of the sample gas in a supersonic jet reduces rotational and vibrational temperatures of the absorber gas down to a few K. Supersonic jet expansion of I_2 and dimethyl-*s*-tetrazine in the laser cavity perpendicular to the optical axis has allowed the recording of ICA spectra at 0.1 K [143]. Cooling of NO_2 [144] and CH_4 [145] molecules down to 4 K demonstrated very strong suppression of the absorption from hot bands such that the identification of the absorbing vibrational band has been accomplished.

Formation, excited-state dynamics, and dissociation of noble gas (He, Ar, Kr, and Xe) van der Waals complexes of I_2 formed in a pulsed supersonic jet have been studied by ICAS with a dye laser [146]. Many of the recorded absorption spectra have been identified. Complexes formed with more than one kind of noble-gas atom decay via non-emitting processes which exclude the alternative use of laser-induced fluorescence for this kind of study.

The spectra of the absorption from highly excited states of various small molecules, such as H_2O, HDO, D_2O [22], CO_2, CH_4, C_2HD, NH_3 [106], C_2H_2, HN_3, HCN [107], CH_3OH [26], C_2D_2, CH_3D, N_2O, H_2, ND_3, N_2H_4 [147], and O_3 [141], have been studied with the help of Nd^{3+}-doped glass lasers, and with LiF:F_2^+/F_2^- CCL in the spectral region from 0.9 μm to 1.25 μm. Most spectra were recorded and identified for the first time. These data have allowed one to determine various molecular constants, pressure broadening coefficients, and frequency shifts.

Extension of the ICA technique into the deeper IR has been achieved by using a KCl:Tl^0(1) CCL to measure the molecular absorption of SiH_4, SiH_2Cl_2, and $SiHCl_3$ in the range 1.48–1.545 μm [148], by using a Cr^{4+}:YAG laser for the spectral absorption of atmospheric water in the range 1.38–1.55 μm [42], of a Co:MgF_2 for the absorption of CO_2 at 2 μm [45], and of a KCl:Li F_a(II) CCL to measure H_2O, N_2O and CH_4 at 2.65 μm [43].

10.1.3 Simulation of planetary atmospheres. Methane is present in the atmospheres of all the outer planets of our solar system and of the natural satellites of Saturn and Neptune, and its absorption distinguishes the light reflected from these celestial bodies. These absorption lines characterize the planetary atmospheres with respect to relative methane abundance, atmospheric pressure, and temperature. Spectrometric data may be fitted by data collected from suitably conditioned laboratory gas probes. The small size of an intracavity absorption cell admits precise control of the temperature, pressure, and fractional concentrations in the gas mixture, which is indispensable for this simulating of planetary atmospheres, and for comparison of ICA spectra with planetary absorption spectra [149]. The line intensities of CH_4 and the coefficients of pressure broadening by N_2, H_2, He, and CH_4, as well as pressure-induced line shifts have been measured in the spectral regions around 620, 680, and 720 nm by using various dye lasers with a controlled pulse duration of up to 200 μs, and with short sampling time intervals (1–2 μs), in a broad range of temperatures, from 77 K to 296 K [149, 150]. At this short pulse duration, nonlinear mode coupling is negligible, and the residual inaccuracy of these fits of absorption line profiles is rather small, viz. about 1%–2%. A detailed measurement of this kind has been devoted to the atmosphere of Saturn [151]. ICAS measurements of line intensities of the 648-nm band of NH_3 in suitable samples at low temperatures allow the comparison with planetary spectrograms and the determination of the abundance of ammonia in the planets' atmospheres, of the altitude of water clouds, and of a presumed cloud of ammonium hydrosulfide, as well as variations of the densities from the centre to the limb of the disks of Jupiter and Saturn [152].

10.1.4 Process control and plasma diagnostics. The production of high-quality silicon films for electronic devices, or of diamond-like carbon films requires in situ control of the process of chemical vapour deposition and in situ monitoring, at extremely low levels, the contamination of the feed gases and the residual pollution from the chamber walls during the processing. Both these capabilities are offered by ICAS. Recording the spectra of the SiH_2 radical in the reaction chamber at concentrations in the ppb range in the 550-nm domain has proven the different efficiency of chemical vapour deposition of thin silicon films when starting from differing silicon-containing compounds, for example ethylsilane and diethylsilane [153, 154]. Moreover, various contaminations, that reduce the quality of the silicon film such as water vapour, have been recorded simultaneously. Many efficient ways of in situ controlling technological processes in the chemical industry have not been exploited so far.

Monitoring an electrical discharge is achieved by recording the distorted absorption profiles of neutral atoms and ions. In a helium–cesium plasma generated by a microwave, or in a cw discharge, the diffuse and sharp series of cesium corresponding to the $6P_{1/2}$–$8D_{3/2}$ and $6P_{3/2}$–$8S_{1/2}$ transitions have been studied. One may separate the contribution of electron broadening and derive the electron concentration in the discharge [155].

ICA of excited hydrogen atoms recorded on the H_α lines at 656.5 nm by a DCM dye laser allows one to reveal or control the temperature and population of H*. This control is important, for example, with plasma-enhanced chemical vapour deposition of diamond-structured carbon films using hydrocarbons as source gases [156]. Similar monitoring could be used with the control of other hydrogen-containing plasmas, for example in nuclear fusion.

10.1.5 Atomic absorption. Many atomic species show absorption on electronic transitions in the visible or near IR and can be detected by ICAS. Moreover, supplementary excitation of higher electronics levels, for example by an electrical discharge, helps to increase the number of detectable absorption lines and species. The detection of atomic absorption by ICAS often requires the vaporization of the sample. Inside a laser cavity a sample is easily vaporized by the flame of an acetylene–air burner, with the solution of a suitable salt injected into the air stream [157]. Absorption lines of Na, Li, Sr, Ba, and Cs have been detected with the use of a flash-lamp-pumped pulsed dye laser. The sensitivity of these measurements was limited by the 3-μs pulse duration to $L_{\text{eff}} = 10$ km, and 5×10^5 atoms/cm^3 of Na have been detected [158]. A RF discharge [159], or flame [160], generates dissociated species

as, for example, atomic oxygen. Thanks to the extreme sensitivity, absorption on highly forbidden atomic intercombination lines has shown up in the cavity of a dye laser. Even atoms that are normally found in the solid phase have given rise to absorption spectra, namely when vaporized by a discharge inside the laser cavity [93] where states excited by electron collisions may also contribute to the absorption, in an atomic beam [94], in an electrothermal atomizer [104], or in a plasma, ignited by a second pulsed laser on the surface of the sample [161].

Atomic absorption may be also recorded when the *solution* of a salt is placed inside the laser cavity. However, the width of the ICA lines should not exceed the homogeneous spectral width of both the gain medium and the emission bandwidth of the laser. This requirement holds with the absorption of rare earth ions in solutions, since their inner electronic transitions responsible for absorption in the visible are not strongly broadened by the surrounding solvent. The linewidth of this absorption is about 1 nm. The extinction of solutions of rare earth salts, such as $Eu(NO_3)_3$, $Pr(NO_3)_3$, $NdCl_3$, $HoCl_3$ in water or methanol has been measured with dye lasers of up to 2.5 μs pulse duration [162]. Measurements on other ions, for example, iron, are not as sensitive, since their spectral absorption features are too broad. However, the sensitivity is still higher than that of conventional measurements. For instance, iron has been detected in a solution at the concentration 0.5 ppb [163].

10.1.6 Isotope separation. Broadband laser light with one particular isotopic species inside the cavity is attenuated in the spectral bands of the isotope-shifted absorption; it cannot excite that same isotope in a cell outside the cavity, although the other isotopes will be excited. This feature can be used for isotope separation when the excited species get removed chemically or by photoionization. A typical example is the separation of ^{35}Cl and ^{37}Cl [164], where an enrichment factor of 17 has been achieved. $I^{35}Cl$ inside the cavity locked the laser output off those unwanted output frequencies that excite $I^{35}Cl$, and in the external cell that contained the isotope mixture, $I^{37}Cl$ was selectively excited (see also [17]). The products of the subsequent photochemical reaction were found enriched in ^{37}Cl. Similar arrangements have been used for the separation of isotopes of H, C, O [165], and of ^{235}U [166].

10.2 Time-resolved measurements

The spectral monitoring of transient processes is one of the salient features of ICAS. With studies of reaction kinetics or for sensitive process control, temporal resolution must supplement high spectral sensitivity of detection. The sensitivity of ICA measurements is determined, as shown above, by the laser pulse duration τ, if the operating conditions of the laser are set such that the spectral saturation time t_s exceeds τ. The time resolution is also determined by the duration of the laser pulse τ necessary for the required sensitivity, according to $L_{\text{eff}}/\tau = c$. Indeed, time resolution can be traded in for sensitivity within wide margins, with 10 ns being the shortest practical resolution time. Absorption measurements with an effective absorption path length $L_{\text{eff}} = 1$ km, for example, can be made resolved at time intervals of 3 μs by using, for example, a flash-lamp-pumped dye laser, where the condition $t < t_s$ is always fulfilled. Time-resolved measurements that go along with high sensitivity are especially useful for the detection of excited atoms or molecules, and of transient species such as free radicals generated, for example, by flash photolysis, flames, discharges, or by chemical reactions. Often the reaction kinetics is accessible.

10.2.1 Spectroscopy of free radicals and chemical reactions. Free radicals are stable but very reactive molecules. Collisions with other species as well as with each other may initiate a chemical reaction and destroy them. Free radicals are important intermediate products of many multistage chemical reactions. The study of these reactions makes for the heart of various chemical applications, as atmospheric chemistry, or process control in chemical industry. However, radicals are usually short-living, and their concentration is small. Thus, they can hardly be studied by conventional spectroscopic techniques. Here, ICAS is the most convenient method.

The amide group NH_2 was the first radical to become detected by its absorption in the cavity of a multimode laser [167]. It was obtained by flash photolysis of ammonia, NH_3, in a cell placed in the cavity of a flash-lamp-pumped Rh6G dye laser. The duration of the dye laser pulse – 0.3 μs, ten times less than the duration of the photolysis pulse – allowed for time-resolved detection when the laser pulse was delayed. Both the production of the radicals and their recombination were studied by recording absorption lines of NH_2 at 605 nm with the laser delayed by up to 0.5 s from the photolysis flash. The lifetime of NH_2 was found to be 1 ms. In addition, the same experimental set-up was used for recording the absorption spectrum of the HCO radicals, produced by flash photolysis of acetaldehyde or formaldehyde. The decay time of the HCO radical was found to be 100 μs.

Detailed examinations of the modus and rate of NH_2 decay in reactions with each other, with other molecules, and by collisions with the walls were made in a series of subsequent experiments using flash-lamp-pumped dye lasers with their pulse duration extending from 2 μs to 20 μs [168–173]. A multistage reaction including two intermediate steps has been unravelled by consequently recording the absorption spectra of NH_2 radicals, of HNO radicals, and eventually of stable NO_2 molecules in the same spectral range, 615–620 nm. Figure 23 shows that the NH_2 radicals vanish within 100 μs and generate NHO radicals, whose self-recombination takes place within 1 s [174]. Such measurements on radicals of long lifetime permit substantially higher sensitivity, for example when using a dye laser with 1-ms pulse duration [175]. A comprehensive survey of various multistage reactions pertinent to the photo-oxidation of ammonia has required to unravel the reactions of NH_2 radicals in various gas mixtures including O_2 [168], O_3 [169], SO_2 [170], NO_2 [171], and NO [172], and other relevant atmospheric molecules. The rate constants of 24 principal reactions important for the photochemistry of the atmosphere have been determined in this way [176]. It was found that the presence of ammonia leads to effective decrease of the concentration of nitrogen oxides [173].

NH_2 radicals are also created in electrical discharges. The rotational distribution of NH_2 in the electronic-vibrational ground state has revealed the dynamics of gas heating in a pulsed low-pressure ammonia–neon discharge [177].

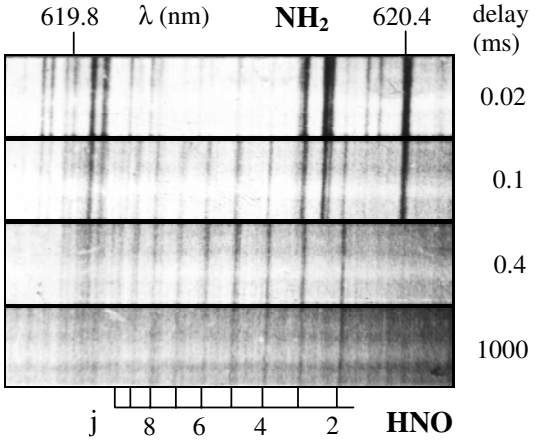

Fig. 23. ICA spectrum photographically recorded by a flash-lamp-pumped dye laser of the photolysis products of a mixture of ammonia with oxygen at various delay times after the photolysis pulse [174]

The photolysis of acetaldehyde was analysed in detail by recording absorption spectra of HCO radicals in the cavity of a cw dye laser with controlled duration of the laser emission [178]. Fast relaxation processes were suitably monitored by 1-μs-long pulses, whereas 100-μs laser pulses were applied for sensitively recording weak absorption. The photolysis was initiated by the fourth harmonic of a Nd:YAG laser at 266 nm with 8-ns pulse length. It was found that absorption on different transitions results in differing decay rates of the radical. This surprising finding derives from the absorption signal decaying both by the recombination of the radicals, and by the relaxation of vibrational excitation: the excited state may either react or vibrationally decay [179]. The number of vibrationally excited radicals and their decay rate depends upon the excited ro-vibrational levels, i.e. upon the wavelength of the photolytic light, and upon the sample pressure [179, 180]. These particular features of the reaction dynamics have to be carefully modelled for correct estimation of the rate constants of the chemical reactions. Moreover, the presence of other molecular species modifies the decay of HCO radicals by opening additional reaction channels [179]. Flash photolysis of acetaldehyde in the presence of NO disclosed a two-stage process [174, 181]: HCO radicals created by the flash react with NO molecules and produce the second intermediate product, HNO radicals, after 100 μs. This radical decays into stable end-products, one of them being NO_2.

Free radicals HCO [182] and CH_2 [183] have been also found in a methane/air flame by ICA detection in the spectral range 620–630 nm. The kinetics of the formation and decay of these radicals and their temperature were measured here along the gas flow as a function of the distance from the burner.

The generation and decay of fluoronitride NF, after flash photolysis of NF_2, in the cavity of a Coumarine 7 dye laser have been recorded in the spectral range around 529 nm at 1.3 μs pulse duration [184]. The lifetime of these radicals in the presence of SF_6 molecules was found to be 15 μs. This exploration approved the feasibility of a chemical laser in the visible on electronic transitions in NF. Another such attempt on BaO, CaO, and SrO required measuring the absorption of the components of certain exothermic reactions, in a flame, of the compositions $Ba + N_2O$, and Ca, $Sr + N_2O + CO$ [185]. The expected gain has not been confirmed so far, however, many absorptive transitions of these oxides were recorded and identified for the first time.

The absorption spectra of several other radicals including HO_2 (1.2–1.27 μm), CH_3O_2 (1.2–1.22 μm), HSO (570–590 nm) have been reported [176]. The spectra of HO_2 and CH_3O_2 radicals were recorded in the cavity of a LiF:F_2^--centre laser [28]. These radicals were generated by flash photolysis of a mixture of methanol, chlorine, and oxygen, or of methane, chlorine and oxygen [176], respectively.

Radicals are also created by a radio-frequency discharge during chemical vapour deposition on surfaces. An example is SiH_2 which is produced in the course of chemical vapour deposition of thin layers of silica [153, 154]. Various boron hydrides have been produced in gas-phase reactions by a RF discharge of B_2H_6 in He or Ar, and their spectra have been analysed in situ in real time under conditions comparable to those used in doping and boriding, as well as in deposition processes involving boron: absorption spectra of BH_2, atomic B, and electronically excited H_2 have been observed by ICAS during chemical vapour deposition [186]. The detection of radicals in the gas phase completes the diagnostics of the RF plasma conditions which control the quality of chemical vapour deposition; they represent an example of advanced process control.

Various diatomic radicals, mostly oxides (MeO) and nitrides (MeN), with Me being a metal atom (Ti, Zr, Nb, Mo, Cr, W), are produced by flash photolysis of hexacarboniles $Me(CO)_6$ [187], or by a pulsed electrical discharge in the gas mixture $MeCl_4 + O_2$ for MeO, and $MeCl_4 + N_2 + Ar$ for MeN [188]. Electronic absorption spectra have been recorded in the visible and near-IR ranges. Many observed absorption bands turned out novel and were successfully assigned, and interatomic potential functions and rotational constants have been determined.

10.2.2 Dynamics of excited states. Time-resolved absorption spectra are crucial for unravelling the dynamics of excited states of atoms and molecules, their evolution of population, lifetime of states and species, energy transfer, and interaction with other species.

The population dynamics of several excited states of Xe in electrical discharge was observed in the cavity of a pulsed LiF:F_2^+-centre laser in the spectral range 880–970 nm [27]. The discharge was probed by the laser at a variable time delay after the pulse that excited the discharge as demonstrated in Fig. 24, and the time resolution in these measurements was 0.2 μs. The lifetime of the lowest metastable state was found to be 400 μs. The same experimental set-up has been used for time-resolved recording absorption spectra of the excimer molecules He_2 in the afterglow of a pulsed discharge [189]. Absorption lines of the P and R branches of the 0-0 vibrational band of the electronic transition $c^3\sum_g^+ - a^3\sum_u^+$ of He_2 have been recorded and assigned. Plots, versus $J(J+1)$, of the rotational line strength normalized by $(2J+1)$ with J being the rotational quantum number ("Hoenl–London plots") have been derived from these data for various time delays and discharge parameters. The rotational energy distribution of the He_2^* molecules, its deviation from thermal equilibrium, and the variation of rotational temperature and metastable population have been derived from these plots as functions of

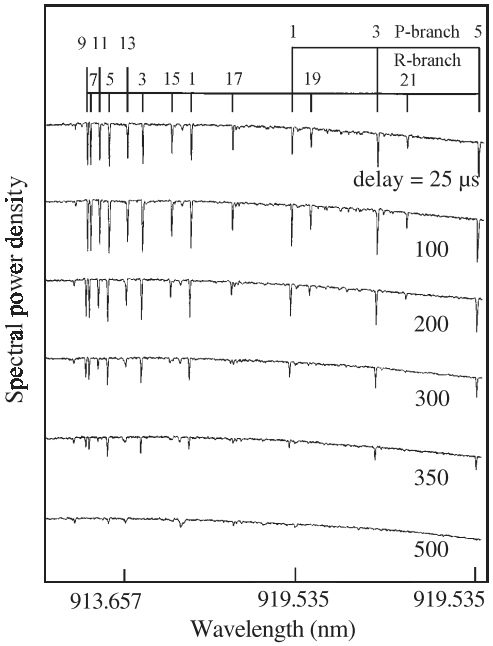

Fig. 24. Absorption spectra of He_2 molecules in an electric discharge plasma of He at 13 mbar, at various times after the termination of the discharge [189]

the time delay in the afterglow. These data reveal the dynamics of the excimer molecules in the discharge. The maximum concentration of He_2 molecules in the lowest excited state shows up 100 μs after the termination of the electrical discharge.

The diagnostics of excited states is especially important for the development of gas lasers. The dynamics of populating the metastable state $A^3 \sum_u^+$ of the nitrogen molecule in the plasma of an electrical discharge has been studied with a Rh6G dye laser of 0.1-μs pulse duration [190]. Substantial time resolution was indispensable since the decay time of this state is about 0.5 μs only. This study permits one to establish the proper conditions for stable operation of a self-sustained volume discharge in a CO_2 laser. The gas composition in a chemical oxygen–iodine laser has been measured by ICAS using a Ti:sapphire laser. The populations of excited oxygen molecules, and the concentration of water vapour, the parameters most important for the efficiency of this laser, have been precisely monitored [191].

10.3 Other applications

10.3.1 Measurements of optical gain. The emission spectrum of a multimode laser is sensitive not only to weak narrow-band extinction in the cavity, but to any other spectral variation of cavity loss that may result, for example, in narrow-band net gain. Therefore, ICAS can be applied to the diagnostics of light amplification in potential laser media. Spectra of gain in various media under different types of excitation have been demonstrated this way. The gain spectrum of the dissociative products of acetylene, C_2H_2, in an electrical discharge was recorded in the spectral region around 1.06 μm using a Nd^{3+}-doped glass laser [192]. Molecular iodine, I_2, was optically excited by an Ar-ion laser, and spectra of its gain were

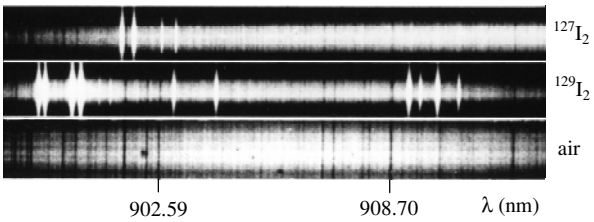

Fig. 25. Photographically recorded emission spectrum of a multimode F_2^+:LiF laser showing bright spectral lines of gain in $^{127}I_2$ (*top*), in $^{129}I_2$ (*centre*), and *dark lines* of atmospheric absorption (*bottom*) [27]

observed at 590 nm in the cavity of a dye laser [193]. When a sample of I_2 was placed in the cavity of a F_2^+:LiF colour centre laser and excited by a pulsed Xe-ion laser, gain was observed at 900 nm [27]. Figure 25 shows an output spectrum of this F_2^+:LiF laser, pumped collinearly through the rear mirror by the same xenon laser that excites also the I_2 inside the cavity of the CCL: part of the pump beam, after passing through the LiF crystal, enters into the intracavity cell filled with the vapour of one of the iodine isotopes $^{127}I_2$ or $^{129}I_2$ and excites it to certain ro-vibrational levels of the first excited electronic state. As a result, the population in many ro-vibrational levels of the excited electronic state is inverted with respect to lower ro-vibrational levels of the electronic ground state and amplifies light in the near IR. Some of these inverted transitions of two isotopes of iodine appear in photographically recorded emission spectra of such a F_2^+:LiF laser in Fig. 25. In contrast to the dark absorption lines, the gain-carrying lines appear bright in the figure. The high gain provided on some of these transitions far exceeds threshold and assures laser oscillation even with the iodine cell alone being the amplifying medium in the cavity [27].

10.3.2 Detection of spectrally narrow light emission. The emission spectrum of a multimode laser is sensitive also to external narrow-band radiation injected into the laser cavity. Under this injection the multimode laser may show, for example, *narrow-band* light emission [194]. This phenomenon may be useful for the detection of very weak back-scattered light, as it is to be detected by LIDAR devices. The minute amounts of retrieved residual light that has been scattered in the turbid medium may trigger a detectable signal on account of the enormous spectral sensitivity [195].

Unfortunately, the very same sensitivity may give rise to parasitic periodicity of the recorded spectra: a minute fraction of the laser output backscattered into the cavity after passing a sheet of glass is capable of impressing a corresponding etalon structure on the laser output spectrum.

10.3.3 Nonlinear light interaction. The extension of ICAS to studies of nonlinear absorption is straightforward. A two-photon absorption line, for example, shows up in ICAS, if the absorber is simultaneously irradiated, in addition to the many modes of the laser, by strong narrow-band light, with any sum frequency of this light and a laser mode being resonant with the absorber. In other words, a photon taken from one of the modes of the broadband laser makes up for the energy defect of a photon of the narrow-band light with respect to the two-photon resonance transition. The excitation of such a line is characterized by a cross section that is resonantly enhanced when a real level whose parity is opposite to the parity of both

ground and excited states comes close to the intermediate virtual level.

A measurement of the cross section for the excitation of a two-photon transition in potassium vapour has included a narrow-band ruby laser and a broadband DOTS dye laser excited by the same ruby laser [196]. In fact, two states, the fine-structure-split resonance levels $^2P_{1/2}$ and $^2P_{3/2}$, enhance the two-photon absorption probability, but can give rise to destructive interference. This interference of indistinguishable pathways from the ground state to the excited state is demonstrated with the detection by ICAS of two-photon absorption in sodium vapour [197], see Fig. 26. A pulsed broadband dye laser was tuned to the frequency range of the Na 3P–5S absorption, and a pulsed narrow-band dye laser close to the 3S–3P resonance transition, say, to the wavelength λ_{12}. One observes, in the spectrum of the broadband laser, an additional absorption line at the wavelength λ_{23}, which varies with λ_{12}, such that their sum frequency equals the two-photon frequency $\nu_{12} + \nu_{23} = \nu_{3S-5S}$. The absorption line at λ_{23} corresponds to the second photon of the two-photon transition. At the particular tuning $\lambda_{12} = 589.40\,\text{nm}$ and $\lambda_{23} = 615.64\,\text{nm}$, the amplitude of the two-photon line vanishes due to destructive interference of the two excitation channels.

If broadband and narrow-band lasers obey $\nu_{12} - \nu_{23} = \pm\nu_{\text{mol}}$, with ν_{mol} being one of the frequencies of a molecular absorber, one observes spectrally selective intracavity gain or loss corresponding to Raman or inverse Raman scattering. In this way inverse Raman scattering of benzene and toluene in the liquid phase in the cavity of a dye laser has been recorded in the range $600\,\text{cm}^{-1} < \nu_{\text{mol}} < 3200\,\text{cm}^{-1}$ [198]. A narrow-band ruby laser at λ_{12} provided the pump light for the Raman process, and its second harmonic the pump light for a dye laser. Thanks to the high sensitivity of the procedure, Raman–Stokes scattering of acetylene at atmospheric pressure in the cavity of a cryptocyanine dye laser at $\lambda_{23} = 804.76\,\text{nm}$ was detected when both Raman scattering and dye laser were excited by the ruby laser at $\lambda_{12} = 694.3\,\text{nm}$. The observed Raman line corresponds to the vibrational transition in acetylene at $\nu_{\text{mol}} = 1957\,\text{cm}^{-1}$ [199].

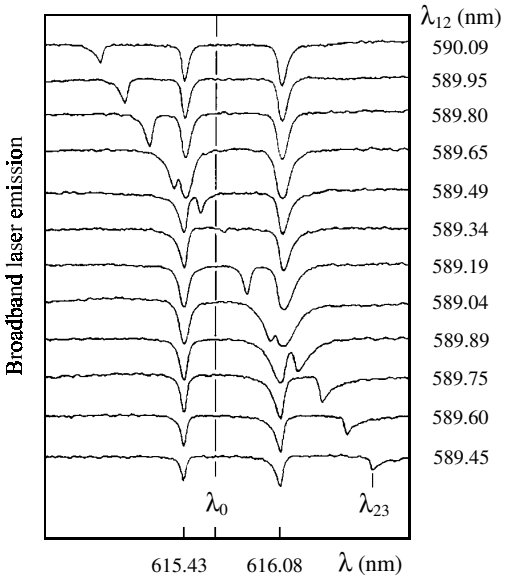

Fig. 26. Absorption spectra of Na vapour, in a broadband dye laser, upon injection of narrow-band light at wavelength λ_{12} stepwise scanned. Two-photon absorption on the transition 3S–5S: the anticorrelated wavelengths λ_{12} and λ_{23} correspond to first and second photons, respectively. The lines at 615.43 nm and 616.08 nm represent single-photon absorption at the 3P–5S transitions [197]

These approaches demonstrate the accessibility of UV or far-IR transitions by sensitive nonlinear techniques involving only visible lasers.

10.3.4 Spectroscopy by attenuated total reflection. If an optical element inside the cavity of a multimode laser is used in a configuration of total reflection, intracavity narrow-band extinction in the evanescent field that spreads outside the reflecting facet of this element is detected in the spectrum of the laser output [200]. Comparative measurements of intracavity absorption of I_2 and NO_2 in a cell and in the evanescent field proved the agreement of the results of this type of ICA measurements [201]. The use of the evanescent field does not require an absorption cell, and it allows one to measure chemically aggressive or scattered microscopic samples. However, due to the exponential decay of the evanescent field with the distance from the surface, the fraction of the total mode volume that the absorber occupies is usually considerably less than in the conventional ICAS configurations. This fraction is substantially increased when guiding the light in the cavity by a fibre, for example by using a fibre laser. In this case the fraction of the evanescent field interacting with the surface-bound absorber may be comparable to the fraction of the field in the fibre core.

11 Spectral resolution of ICAS

In the typical configuration of an ICAS spectrometer shown in Fig. 1 the spectral resolution of a measurement of absorption is ultimately determined by the spectral separation of the laser modes, $c/2L$. In contrast to conventional absorption measurements, however, recorded spectra of ICA represent the signal integrated not over the spectral interval of resolution, but just over the bandwidth of individual laser modes, β, which is much less than $c/2L$. Therefore, the ICA spectrum is not obtained as the usual convolution of the transmission spectrum of the sample with the apparatus function of the spectrometer, but it is represented by the set of transmission values that result from probing the absorber at fixed spectral positions. If the absorption feature of the sample is larger than the mode separation, it is well reproduced in ICAS measurements. However, if this feature is smaller than that mode separation, its reproduction is uncertain. It may even disappear entirely from the ICA spectrum as, for example, a narrow absorption line that is situated between two adjacent laser modes.

This specific characteristic of ICA measurements is schematically demonstrated in the example of Fig. 27. The absorption spectrum of the sample is assumed to consist of two absorption lines of different strengths and linewidths (Fig. 27a). The emission spectrum of a laser with ICA reproduces the absorption of the sample only at the frequencies of the oscillating laser modes, as indicated by the length of fat vertical lines in Fig. 27b. The thin line shows the superimposed transmission spectrum of the sample. The imaging of the absorption spectrum by the laser modes is insufficient, since the spectral separation of the modes exceeds the

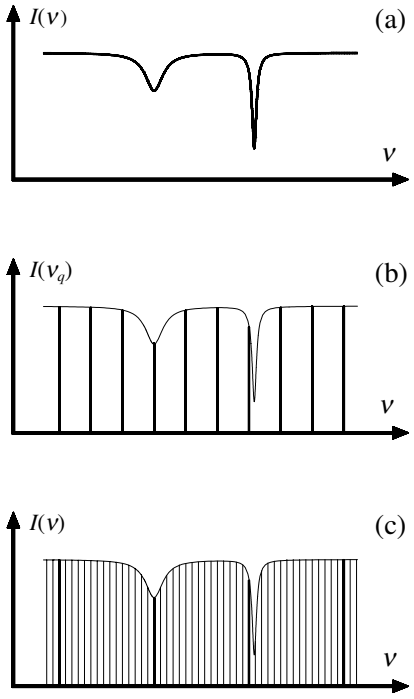

Fig. 27a–c. Schematic demonstration of ICA measurements: **a** Absorption spectrum of a sample. **b** Emission spectrum of a laser with ICA, comprising a set of oscillating laser modes whose power is indicated by the length of the vertical lines. **c** Succesive spectral positions of the emitting laser modes obtained by synchronously scanning the cavity length and intracavity etalon. *Fat lines* represent the initial mode positions. A *thin line* in **b** and **c** shows the transmission spectrum of the sample obtained during the scan

linewidth of the sample's absorption. Note that the weak absorption line perfectly overlaps with the laser mode and shows even a larger ICA signal than the second absorption line which is stronger but does not match a laser mode.

The spectral separation of longitudinal modes in a typical laser is usually smaller than the linewidth of gaseous absorption under normal conditions. With a 1-m-long resonator, for example, it amounts to $0.005\,\mathrm{cm}^{-1}$, or 150 MHz. This resolution satisfies measurements of molecular absorption lines with collisionally broadened profiles, say, at atmospheric pressure, which are typically 3 GHz wide.

11.1 ICAS of high resolution

The implementation of this resolution requires the application of spectrometers with very high resolving power, i.e., $\nu/\Delta\nu = 4 \times 10^6$. Typically the resolution of standard grating spectrometers extends from 10^4 through 10^6. Thus, the spectral resolution of ICAS is usually determined by the spectrometer used. However, the spectral resolution can approach the value of mode separation even if the resolution $\Delta\nu$ of the spectrometer is insufficient. For this purpose an etalon, whose base d is much smaller than the cavity length L, is placed in the cavity such that only one oscillating laser mode is left over per free spectral range of the etalon, and the corresponding spectral modulation is resolved by the spectrometer, $\Delta\nu < c/2d$. When the etalon is scanned across the emission spectrum of the laser, for example by tilting it, the laser emission jumps from one laser mode to the next one, and

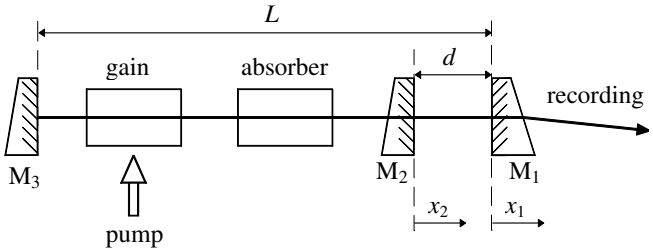

Fig. 28. Schematic experimental set-up used for ICAS measurements with high spectral resolution. The laser cavity includes gain, absorber, two cavity mirrors M1 and M3 and an etalon mirror M2. Mirrors M1 and M2 are synchronously translated by x_1 and x_2 by piezoceramic translators

so on [202]. Finally, the total emission spectrum of the laser is obtained by combining records spectrally shifted by $c/2L$ increments, that have been made while scanning the etalon over one free spectral range.

Better spectral resolution is achieved by synchronously scanning both the intracavity etalon, and the cavity resonances [203]. The scanning speed of the cavity length must equal d/L times that of the etalon. Thus, the spectral positions of the emitting laser modes scan continuously across the emission spectrum, as explained in Fig. 27c. Dark lines represent the initial positions of oscillating modes in the laser. The spectral separation between these modes is much larger than in Fig. 27b due to mode selection by the intracavity etalon. Thin vertical lines represent the successive values of position and strength of laser modes measured by this synchronous fine tuning of the etalon spacing and the cavity length. The spectral features of the absorption sample are well reproduced in this record. The spectral increment may be set as small as necessary for the required spectral resolution. Now, the ultimate spectral resolution is in fact determined by the emission bandwidth of the laser modes, β.

Figure 28 schematically shows a set-up used for recording ICA with high spectral resolution [203]. The laser cavity includes gain, absorber, and two mirrors M1 and M3, as in Fig. 1, but an additional etalon mirror M2, which is just a glass substrate with 4% reflection. This weak etalon suffices for suppressing all but one laser mode in each of its free spectral ranges, since the laser is very sensitive to selective loss in the cavity. The rear side of the substrate M2 subtends the Brewster angle in order to avoid a parasitic etalon. Both output coupler M1 and etalon M2 are placed on piezo elements and translated by a ramp voltage. In order to achieve a spectral record of the entire range of laser emission, all the active modes have to be scanned at least over one free spectral range of the etalon. This is achieved by shifting the output coupler M1 by $x_1 = \lambda L/2d$. At the same time, the etalon spacing must be increased by $x_1 - x_2 = \lambda/2$, as accomplished by shifting the mirror M2 by $x_2 = (\lambda L/2d) - \lambda/2$. The speeds of mirrors M1 and M2 are related as $\dot{x}_2/\dot{x}_1 = 1 - d/L$ in order to warrant synchronism.

In an experiment demonstrating high spectral resolution and sensitivity of ICAS, a Ne discharge has been probed in the cavity of a cw Rh6G dye laser, pumped by a pulse-modulated Ar-ion laser. The duration of laser pulses was 1 ms. An etalon was formed by the output coupler M1 and the mirror substrate M2 being separated by $d = 4.5$ cm.

Figure 29 shows the absorption line of Ne at 576.442 nm; it represents the first ICAS measurement with high spec-

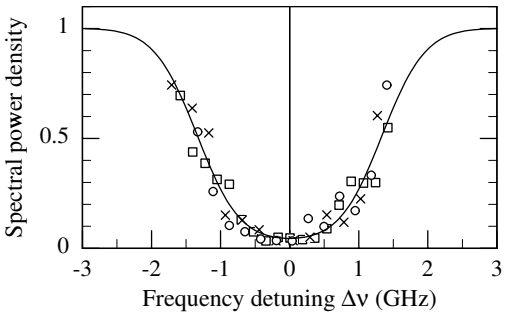

Fig. 29. Absorption line of Ne at 576.442 nm in a cw discharge recorded by ICAS with high spectral resolution. The *solid line* is a Doppler-fit to three sets of experimental data

tral resolution. The pressure of Ne is 1 mbar, and the absorption line is Doppler-broadened with 0.88 GHz (HWHM) linewidth at 470 K, whereas the spectral resolution of the spectrograph is $\Delta\nu = 0.42$ GHz (HWHM). The line profile has been recorded within one free spectral range of the etalon, 3.4 GHz. The polychromator operated in the monochromator mode with a rectangular apparatus function whose spectral width is $\Delta\nu = 3.2$ GHz, slightly smaller than the free spectral range of the etalon. The output signal was detected by a photomultiplier, and the spectral distance between subsequent data points is 175 kHz. Averaging over 50 spectral scans reduces the spectral noise. The solid line in Fig. 27 is a fit to the experimental data by a Doppler profile. The linewidth of the fit is 0.9 GHz (HWHM), which is in good agreement with the expected value. Recording in a broader spectral range would require for detection a diode array instead of a photomultiplier.

11.2 The limits of resolution

The ultimate spectral resolution of the above approach equals the bandwidth of a laser mode. If spontaneous emission is the only perturbation of coherence in the laser, this bandwidth might be just a small fraction of 1 Hz [204]. However, as shown above, other types of perturbation of light coherence usually dominate the multimode laser. They determine the spectral saturation time as well as the bandwidth of the laser modes. The corresponding relation of spectral saturation time and spectral bandwidth of the laser modes can be expressed in terms of multiple-beam interference of light waves that decay under the action of perturbation X_q [50]. The spectral distribution of the light power within a mode is described by Airy's formula [1]

$$I = I_0 \frac{1}{1 + F \sin^2 \Delta\varphi/2}\,, \tag{45}$$

where $\Delta\varphi = 2L\Delta\omega/c$ is the phase difference of interfering waves of frequency separation $\Delta\omega$ that is accumulated after one round trip in the cavity, and $F = 4(1-\delta)/\delta^2$, with δ being the relative loss of light after one path through the cavity due to perturbation X_q. This loss is calculated from (31) as $\delta = \dot{M}t/M_q^{\mathrm{s}} = X_q L/M_q^{\mathrm{s}} c$. If $\delta \ll 1$, we obtain $F = (2/\delta)^2 = (2M_q^{\mathrm{s}} c/LX_q)^2$. In this approximation, the sine function is replaced by its argument, and the final spectral distribution of the light power $I(\omega)$ is identified as the Lorentzian shape $I_0/[1 + (\frac{\omega-\omega_q}{1/2\beta})^2]$. The spectral width (FWHM) of this profile, β , is calculated with (45), by setting $I = \frac{1}{2} I_0$,

$$\beta = \frac{X_q}{M_q^{\mathrm{s}}}\,. \tag{46}$$

Taking into account that $t_{\mathrm{s}} = M_q^{\mathrm{s}}/X_q$ (see (36)), we find the general relationship

$$\beta t_{\mathrm{s}} = 1\,. \tag{47}$$

This result characterizes the universal relationship between the spectral width of the light emission in an individual laser mode which represents the ultimate spectral resolution of ICAS, and the saturation time of the spectral laser dynamics which represents the ultimate sensitivity of ICAS.

The above result shows that increasing perturbation of the laser light in the cavity causes the decrease of the spectral saturation time of the laser dynamics, *and* the increase of the spectral bandwidth of the individual laser modes. Consequently, the fundamental limit of the spectral bandwidth of laser modes, as calculated by Schawlow and Townes [204] with the assumption of spontaneous emission as the only perturbation, is inaccessible with most lasers. Instead, the spectral bandwidth of the laser modes is determined by the dominant perturbation of laser coherence, for example Rayleigh scattering, or by nonlinearities, and Schawlow's and Townes's result must be generalized according to (46).

12 ICAS with a single-mode laser

Sometimes absorption inside a laser cavity does not meet the principal condition for ICAS-related high sensitivity, namely that the linewidth of intracavity absorption must not exceed the spectral width of the homogeneously broadened gain. This situation is met, for example, when a single-mode laser is used for intracavity measurements [205–207], or when the emission bandwidth of a multimode laser is smaller than the absorber linewidth [208]. We qualify these situations as "single-mode ICAS", in contrast to multimode ICAS, as discussed so far, where the condition for high sensitivity holds.

The sensitivity of single-mode lasers to ICA is significantly below that of multimode lasers. Figure 30 demonstrates the two situations and their principal difference. It shows the spectral distribution of the cavity loss, $\gamma(\nu)$, including an ICA line, and the spectral profiles of the gain in both

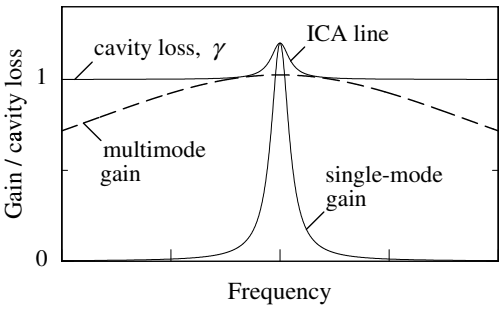

Fig. 30. Gain of a multimode (*dashed line*) and single-mode (*solid line*) laser in the presence of narrow-line ICA in the laser

laser types. In the stationary state, the laser gain is always set by the mode with the smallest net loss (see (20)). In the multimode laser the gain is set by the modes without ICA, as shown by the dashed line. Therefore, the loss by ICA *is left uncompensated* by the gain, and light emission drops in the spectral range of ICA absorption. On the other hand, the gain of a single-mode laser is set by the loss in this particular mode. When tuned to the centre of the ICA line it equals the total cavity loss including γ and ICA, as shown in Fig. 30 by the solid line. In this case, ICA *is compensated* by increased gain, and the reduction of output power is insignificant.

Single-mode ICAS shows increased sensitivity at the pump rate being reduced close to threshold, in contrast with multimode ICAS: At the reduced pumping, the laser can compensate just partially the ICA loss by additional gain. This phenomenon has been described by simplified laser equations neglecting spontaneous emission. Such calculations show indeed qualitatively higher sensitivity at lower pump rate, although the sensitivity grows infinitely when approaching laser threshold [1, 205, 209]. The inclusion of spontaneous emission into a set of laser equations based on field amplitudes has provided a more realistic result and shown sensitivity saturating near threshold [210].

The derivation of the spectral sensitivity of single-mode ICAS requires, in the first place, suitable modelling of spontaneous emission. Restriction of the above rate-equation model to one laser mode is sufficient for this purpose: The stationary solutions of rate equations (10) and (11) are

$$M = \frac{1}{2}\left(\frac{P}{\gamma} - \frac{A}{B}\right) + \sqrt{\frac{1}{4}\left(\frac{P}{\gamma} - \frac{A}{B}\right)^2 + \frac{P}{\gamma}}\,, \tag{48}$$

$$N = \left[\frac{1}{2}\left(\frac{A}{P} + \frac{B}{\gamma}\right) + B\sqrt{\frac{1}{4P^2}\left(\frac{P}{\gamma} - \frac{A}{B}\right)^2 + \frac{1}{\gamma P}}\right]^{-1}\,. \tag{49}$$

Intracavity absorption with the coefficient κ increases the cavity loss by

$$\Delta\gamma = \kappa c\,. \tag{50}$$

With $P_{\mathrm{th}} = A\gamma/B$, and $P = \eta P_{\mathrm{th}}$, we obtain, for $\eta \gg 1$, the photon number

$$M = \frac{A}{B}\left(\eta\frac{\gamma}{\gamma + \Delta\gamma} - 1\right)\,, \tag{51}$$

and the inversion

$$N = \frac{\gamma + \Delta\gamma}{B}\,. \tag{52}$$

Here, the relative pump rate is defined for the cavity with no intracavity absorber ($\kappa = 0$).

Equation (51) shows the decrease of the laser output power by intracavity absorption. The effective absorption path length L_{eff} is easily calculated from this equation using (5) and (22):

$$L_{\mathrm{eff}} = \frac{c}{\Delta\gamma}\ln\frac{M(\gamma)}{M(\gamma + \Delta\gamma)} \cong \frac{\eta}{\eta - 1}\frac{c}{\gamma}\,. \tag{53}$$

If T is the fractional loss of light per round trip in the cavity, we get from (53), for $\eta \gg 1$,

$$L_{\mathrm{eff}} \cong \frac{c}{\gamma} = \frac{2L}{T}\,. \tag{54}$$

Comparison with (28) shows that the sensitivity of single-mode ICAS fails to meet the sensitivity of multimode ICAS by the factor M_q^s, i.e. the photon number in the absorbed laser mode, which usually amounts to many orders of magnitude.

Sensitivity enhancement ξ over conventional one-way absorption is defined as the ratio of the effective absorption length and the length of the intracavity absorber. If the entire cavity is filled with the absorber,

$$\xi = \frac{L_{\mathrm{eff}}}{L}\,. \tag{55}$$

As a numerical example, we give the absorption signal obtained in the output of a strongly pumped single-mode dye laser with $L = 1$ m and $T = 0.01$, and filled with an absorber: it is 200 times stronger than with the absorber outside the cavity, $\xi = 2/T = 200$.

Close to laser threshold the approximate solutions in (51)–(53) do not hold, and the exact solution of (48) and (49) should be used. Figure 31 (top) shows the calculated output power of a cw dye laser calculated with (48) versus the pump rate, for nine different values of cavity loss, $\gamma = \gamma_0 + \kappa c$, with γ_0 being the internal cavity loss, and κ the extinction caused by the additional intracavity absorber. The laser parameters used for these data are $L = 1$ m, $A = 1.7 \times 10^8\ \mathrm{s}^{-1}$, $B = 10^{-2}\ \mathrm{s}^{-1}$, $\gamma = 1.5 \times 10^6\ \mathrm{s}^{-1}$ (1% loss per cavity round trip). The pump rate η refers to the threshold value $P_{\mathrm{th}} = 2.55 \times 10^{16}\ \mathrm{s}^{-1}$ of the laser with $\kappa = 0$. The extra loss is distributed over the cavity length and corresponds to absorption coefficients from 1×10^{-9} through $8 \times 10^{-9}\ \mathrm{cm}^{-1}$.

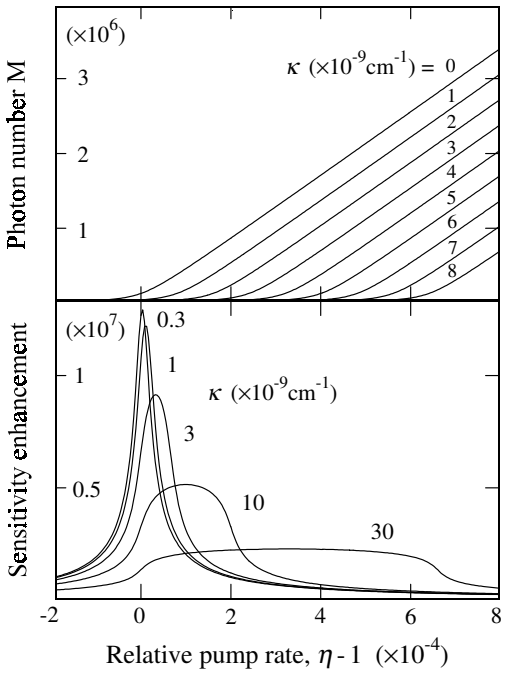

Fig. 31. ICAS with single-mode laser: output of a laser (*top*) and sensitivity enhancement (*bottom*) as function of the pump rate, $\eta - 1$, at different values of ICA absorption κ

Figure 31 (top) reveals that the fractional variation of the laser power due to the incremental extra loss in the cavity is particularly high close to the laser threshold ($\eta \cong 1$). The sensitivity enhancement ξ calculated from these data is shown in Fig. 31 (bottom) as a function of the pump rate for five values of the absorption coefficient κ. The maximum value of sensitivity enhancement, $\xi = 1.3 \times 10^7$ is obtained near threshold within $\kappa < 10^{-9}\,\mathrm{cm}^{-1}$. It corresponds to the effective absorption path length $L_{\mathrm{eff}} = 1.3 \times 10^4\,\mathrm{km}$. This high sensitivity is hardly established in practice: the required residual instability of the pump power must be as low as 10^{-5}, for example, and sensitivity and resolution of the detection of output power must be as high as to discriminate 10 nW. A monochromator must filter spontaneous emission in the other modes except when the laser displays narrow spectral gain, as for example a CO_2 laser [205], or an Ar-ion laser [206]. If the output of more than one mode is detected, the sensitivity decreases.

Single-mode ICAS can be also used for the detection of gain. A few hundredths of a percent of gain by excited CO molecules has been detected inside the cavity of a single mode CO laser [211].

Although the sensitivity of single-mode ICAS is smaller than that of multimode ICAS, it still exceeds the sensitivity of conventional absorption spectroscopy. It may be useful for measurements of broadband absorbers, and it requires simple means of detection only. Certainly it is suitable for addressing special problems of light absorption.

Even a two-mode laser shows high sensitivity to intracavity absorption, if just one mode feels this absorption [212]. The laser gain is set by the mode unaffected by ICA, and the other mode exponentially decays, like the modes in a multimode laser. Such a device might be also applied to ICAS. However, as a matter of fact, a laser with broadband gain operates single-mode if the other modes are strongly suppressed, but multimode if the suppression is insufficient. An attempt to build a two-mode laser with a binary resonator, but with the same active medium shared by the modes [213] was unsuccessful since the loss in both cavities could not be made balanced precisely. The tolerance to the residual difference depends upon the required sensitivity, and is as small as $1/L_{\mathrm{eff}}$, which was never accomplished.

Other variations of single-mode intracavity spectroscopy have been furnished with the detection of fluorescence [214, 215], photoacoustic signals [105, 216], or saturation [7] inside the laser cavity. Here, the detected signal is enhanced, over conventional spectroscopy, by the power in the laser cavity much exceeding the output power. Thus, the enhancement of sensitivity follows the power enhancement and would be on the order of 100.

13 Summary

This review has dealt with the fundamental properties of multimode lasers. The extreme sensitivity of their emission spectra to minute intracavity absorption is the basis for laser intracavity absorption spectroscopy. Depending on the laser type and operation parameters, the sensitivity L_{eff} of this technique is limited by the duration of the laser pulse, or in cw operation by various perturbations of laser coherence, in particular spontaneous emission, Rayleigh scattering, and nonlinear mode-coupling. Measurements of absorption made by ICAS allow for accurate determination of extremely small absorption coefficients, of wavelength positions, and of the broadening of weak absorption lines in gases. The detectable concentration of an absorber is further reduced by optimizing the detectivity $(K_{\mathrm{min}})^{-1}$ of the recorded laser light.

The ultimate spectral resolution β of ICAS measurements is determined by the emission bandwidth of laser modes, which in turn is determined by the same perturbations as the sensitivity, such that

$$\beta = \frac{c}{L_{\mathrm{eff}}}\,. \tag{56}$$

The capability of ICAS is exploited to the ultimate by the recording of transient processes, when high time resolution is required in addition to high spectral sensitivity. Time resolution is restricted by the laser pulse duration τ (if $\tau < t_{\mathrm{s}}$) that is necessary to achieve the required sensitivity,

$$\tau = \frac{L_{\mathrm{eff}}}{c}\,. \tag{57}$$

ICAS is the only sensitive spectroscopic technique providing parallel spectral recording. The laser emission yields as much simultaneous spectral information as modes are oscillating.

The sensitivity of single-mode ICAS, $L_{\mathrm{eff}}^{\mathrm{sm}}$ is higher than the sensitivity of conventional detection of absorption, although much lower than that of multimode ICAS, $L_{\mathrm{eff}}^{\mathrm{mm}}$. At a high pump rate $\eta \gg 1$, these two figures of sensitivity relate as

$$L_{\mathrm{eff}}^{\mathrm{mm}} = M_q L_{\mathrm{eff}}^{\mathrm{sm}}\,. \tag{58}$$

Many lasers have been tested for their suitability for multimode ICAS. The highest sensitivity so far has been demonstrated with a cw dye laser. It corresponds to the effective absorption path length $L_{\mathrm{eff}} = 70\,000\,\mathrm{km}$. The various examples presented in this review show the benefits and resources of the ICAS technique with respect to many practical applications. The development of new compact multimode lasers, the optimization of their parameters, and improved data processing will make this technique pervade, in the near future, many areas of applied spectroscopy.

Acknowledgements. This work was supported by the Deutsche Forschungsgemeinschaft, and in part by the Volkswagen-Stiftung, and the Hamburgische Wissenschaftliche Stiftung. The authors wish to thank J. Sierks for numerical data calculation.

References

1. W. Demtröder: *Laser Spectroscopy*, Springer Ser. Chem. Phys., Vol. 5 (Springer, Berlin, Heidelberg 1988)
2. S. Mukamel: *Principles of Nonlinear Optical Spectroscopy* (Oxford University Press, New York 1995)
3. A.C. Tam: In *Ultrasensitive Laser Spectroscopy*, ed. by D.S. Kliger (Academic Press, New York 1983) p. 15
4. M.W. Sigrist (Ed.): *Air Monitoring by Spectroscopic Techniques* (Wiley, New York 1994)
5. T. Platz, W. Demtröder: Chem. Phys. Lett. **294**, 397 (1998)
6. J.A. Silver: Appl. Opt. **31**, 707 (1992)

7. J. Ye, L.-S. Ma, J.L. Hall: J. Opt. Soc. Am. B **15**, 6 (1998)
8. J.A. Curcio, L.F. Drummeter, G.L. Knestrick: Appl. Opt. **3**, 1401 (1964)
9. H. Edner, P. Ragnarson, S. Spännare, S. Svanberg: Appl. Opt. **32**, 327 (1993)
10. J.U. White: J. Opt. Soc. Am. **32**, 285 (1942)
11. J. Ballard, K. Strong, J.J. Remedios, M. Page, W.B. Johnston: J. Quant. Spectrosc. Radiat. Transfer **52**, 677 (1994)
12. A. O'Keefe, D.A.G. Deacon: Rev. Sci. Instrum. **59**, 2544 (1988)
13. D. Romanini, K.K. Lehmann: J. Chem. Phys. **99**, 6287 (1993)
14. L.A. Pakhomycheva, E.A. Sviridenkov, A.F. Suchkov, L.V. Titova, S.S. Churilov: Pis'ma Zh. Eksp. Teor. Fiz. **12**, 60 (1970) [JETP Lett. **12**, 43 (1970)]
15. T.P. Belikova, E.A. Sviridenkov, A.F. Suchkov, L.V. Titova, S.S. Churilov: Zh. Eksp. Teor. Fiz. **62**, 2060 (1972) [Sov. Phys. JETP **35**, 1076 (1972)]
16. E.A. Sviridenkov: Proc. SPIE **3342**, 1 (1998)
17. T.W. Hänsch, A.L. Schawlow, P.E. Toschek: IEEE J. Quantum Electron. **QE-8**, 802 (1972)
18. P.E. Toschek, V.M. Baev: In *Lasers, Spectroscopy and New Ideas*, ed. by W.M. Yen, M.D. Levenson (Springer, Berlin, Heidelberg 1987) pp. 89–111
19. V.M. Baev, P.E. Toschek: Proc. SPIE **1715**, 381 (1992)
20. J. Sierks, T. Latz, V.M. Baev, P.E. Toschek: Proceedings of the 1996 European Quantum Electronics Conference (EQEC'96), 8–13 September 1996, Hamburg, p. 100, QWB6
21. T.P. Belikova, B.K. Dorofeev, E.A. Sviridenkov, A.F. Suchkov: Kvant. Elektron. **2**, 1325 (1975) [Sov. J. Quantum Electron. **5**, 722 (1975)]
22. A.D. Bykov, V.P. Lopasov, Yu.S. Makushkin, L.N. Sinitsa, O.N. Ulenikov, V.E. Zuev: J. Mol. Spectrosc. **94**, 1 (1982)
23. N.C. Peterson, M.J. Kurylo, W. Braun, A.M. Bass, R.A. Keller: J. Opt. Soc. Am. **61**, 746 (1971)
24. E.N. Antonov, V.G. Koloshnikov, V.R. Mironenko: Opt. Commun. **15**, 99 (1975)
25. V.M. Baev, T.P. Belikova, E.A. Sviridenkov, A.F. Suchkov: Zh. Eksp. Teor. Fiz. **74**, 43 (1978) [Sov. Phys. JETP **47**, 21 (1978)]
26. V.M. Baev, V.F. Gamalij, B.D. Lobanov, E.F. Martynovich, E.A. Sviridenkov, A.F. Suchkov, V.M. Khulugurov: Kvant. Elektron. **6**, 92 (1979) [Sov. J. Quantum Electron. **9**, 51 (1979)]
27. V.M. Baev, H. Schröder, P.E. Toschek: Opt. Commun. **36**, 57 (1981)
28. V.P. Bulatov, Y.V. Matyagin, N.A. Raspopov, A.N. Savchenko, E.A. Sviridenkov: Kvant. Elektron. **16**, 1357 (1989) [Sov. J. Quantum Electron. **19**, 875 (1989)]
29. D.A. Gilmore, P. Vujkovic Cvijin, G.H. Atkinson: Opt. Commun. **77**, 385 (1990)
30. J. Sierks, J. Eschner, V.M. Baev, P.E. Toschek: Opt. Commun. **102**, 265 (1993)
31. A. Kachanov, A. Charvat, F. Stoeckel: J. Opt. Soc. Am. B **12**, 970 (1995)
32. V.M. Baev, J. Eschner, E. Paeth, R. Schüler, P.E. Toschek: Appl. Phys. B **55**, 463 (1992)
33. V.L. Velichanskij, S.E. Vinogradov, E.A. Sviridenkov, G.G. Kharisov: Pis'ma Zh. Eksp. Teor. Fiz. **61**, 87 (1995) [JETP Lett. **61**, 91 (1995)]
34. R. Böhm, A. Stephani, V.M. Baev, P.E. Toschek: Opt. Lett. **18**, 1955 (1993)
35. E.N. Antonov, P.S. Antsyferov, A.A. Kachanov, V.G. Koloshnikov: Opt. Commun. **41**, 131 (1982)
36. P. Vujkovic Cvijin, W.K. Wells, D.A. Gilmore, J. Wu, D.M. Hunten, G.H. Atkinson: Appl. Opt. **31**, 5779 (1992)
37. A.A. Kachanov, T.V. Plakhotnik: Opt. Commun. **47**, 257 (1983)
38. F. Stoeckel, M.-A. Melieres, M. Chenevier: J. Chem. Phys. **76**, 2191 (1982)
39. V.M. Baev, T.P. Belikova, S.A. Kovalenko, E.A. Sviridenkov, A.F. Suchkov: Kvant. Elektron. **7**, 903 (1980) [Sov. J. Quantum Electron. **10**, 517 (1980)]
40. K. Strong, T.J. Johnson, G.W. Harris: Appl. Opt. **36**, 8533 (1997)
41. A. del Olmo, C. Domingo, J.M. Orza, D. Bermejo: J. Mol. Spectrosc. **145**, 323 (1991)
42. D.A. Gilmore, P. Vujkovic Cvijin, G.H. Atkinson: Opt. Commun. **103**, 370 (1993)
43. V.M. Baev, V.P. Dubov, A.N. Kireev, E.A. Sviridenkov, D.D. Toptygin, O.I. Yushchuk: Kvant. Elektron. **13**, 1708 (1986) [Sov. J. Quantum Electron. **16**, 1121 (1986)]; G. Litfin, V.M. Baev: Atmos. Opt. (USSR) **1**, 25 (1988)
44. N.A. Raspopov, E.A. Sviridenkov, A.N. Kolerov, O.I. Yushchuk: Kvant. Elektron. **26**, 219 (1999) [Quantum Electron. **29**, 219 (1999)]
45. M.P. Frolov, Y. P. Podmar'kov: Opt. Commun. **155**, 313 (1998)
46. R.A. Keller, N.S. Nogan, D.S. Bomse: Appl. Opt. **22**, 3331 (1983)
47. E.F. Zalewski, R.A. Keller, C.T. Apel: Appl. Opt. **20**, 1584 (1981)
48. A.E. Siegman: *Lasers* (University Science Books, Mill Valley, CA 1986)
49. H. Haken: *Light*, Vol. 2: *Laser Light Dynamics* (North-Holland, Amsterdam 1985)
50. T. Latz, F. Aupers, V.M. Baev, P.E. Toschek: Opt. Commun. **156**, 210 (1998)
51. J. Sierks: PhD Thesis, Hamburg University, 1995
52. J. Eschner: PhD Thesis, Hamburg University, 1993
53. V.M. Baev, J. Sierks, T. Latz, J. Hünkemeier, P.E. Toschek: In *Laser Spectroscopy, XIII International Conference*, ed. by Z. Wang, Z. Zhang, Y. Wang (World Scientific, Singapore 1998) pp. 349–351
54. J. Hünkemeier, R. Böhm, V.M. Baev, P.E. Toschek: unpublished
55. S.J. Harris, A.M. Weiner: J. Chem. Phys. **74**, 3673 (1981); S.J. Harris: Opt. Lett. **7**, 497 (1982); S.J. Harris: Appl. Opt. **23**, 1311 (1984)
56. Y.M. Aivazyan, V.M. Baev, V.V. Ivanov, S.A. Kovalenko, E.A. Sviridenkov: Kvant. Elektron. **14**, 279 (1987) [Sov. J. Quantum Electron. **17**, 168 (1987)]
57. A.E. Siegman: Appl. Phys. B **60**, 247 (1995)
58. S. Wu, A. Yariv, H. Blauvelt, N. Kwong: Appl. Phys. Lett. **59**, 1156 (1991)
59. M.N. Zervas, R.I. Laming: IEEE J. Quantum Electron. **QE-31**, 468 (1995)
60. S.E. Vinogradov, A.A. Kachanov, S.A. Kovalenko, E.A. Sviridenkov: Pis'ma Zh. Eksp. Teor. Fiz. **55**, 560 (1992) [JETP Lett. **55**, 581 (1992)]
61. J. Sierks, V.M. Baev, P.E. Toschek: Opt. Commun. **96**, 81 (1993)
62. H. Atmanspacher, H. Scheingraber, V.M. Baev: Phys. Rev. A **35**, 142 (1987)
63. J. Sierks, T. Latz, V.M. Baev, P.E. Toschek: Phys. Rev. A **57**, 2186 (1998)
64. M. Sargent III, M.O. Scully, W.E. Lamb, Jr.: *Laser Physics* (Addison-Wesley, Reading, MA 1974)
65. I. McMackin, C. Radzewicz, M. Beck, M.G. Raymer: Phys. Rev. A **38**, 820 (1988)
66. S.A. Kovalenko, S.P. Semin, D.D. Toptygin: Kvant. Elektron. **18**, 451 (1991) [Sov. J. Quantum Electron. **21**, 407 (1991)]
67. D.L. Hart, A. Judy, T.A.B. Kennedy, R. Roy, K. Stoev: Phys. Rev. A **50**, 1807 (1994)
68. S.E. Hodges, M. Munroe, J. Cooper, M.G. Raymer: J. Opt. Soc. Am. B **14**, 191 (1997)
69. W. Brunner, H. Paul: Opt. Quantum Electron. **12**, 393 (1980)
70. B.I. Stepanov, A.N. Rubinov, M.V. Belokon: Zh. Prikl. Spektrosk. **24**, 423 (1974)
71. K. Tohma: Opt. Commun. **15**, 17 (1975)
72. S.A. Kovalenko, S.P. Semin: Opt. Commun. **71**, 189 (1989)
73. T. Latz, J. Sierks, V.M. Baev, P.E. Toschek: unpublished
74. V.F. Gamalij, E.A. Sviridenkov, D.D. Toptygin: Kvant. Elektron. **15**, 2457 (1988) [Sov. J. Quantum Electron. **18**, 1541 (1988)]
75. V.M. Baev, J. Eschner, A. Weiler: Appl. Phys. B **49**, 315 (1989)
76. V.R. Mironenko, V.J. Yudson: Opt. Commun. **34**, 397 (1980)
77. S.A. Kovalenko: Kvant. Elektron. **8**, 1271 (1981) [Sov. J. Quantum Electron. **11**, 759 (1981)]
78. B. Das, G.M. Alman, N.B. Abraham, E.B. Rockower: Phys. Rev. A **39**, 5153 (1989)
79. Y.M. Aivazyan, V.M. Baev, T.P. Belikova, S.A. Kovalenko, E.A. Sviridenkov, O.I. Yushchuk: Kvant. Elektron. **13**, 612 (1986) [Sov. J. Quantum Electron. **16**, 397 (1986)]
80. H. Atmanspacher, H. Scheingraber: Phys. Rev. A **34**, 253 (1986)
81. M. Beck, I. McMackin, M.G. Raymer: Phys. Rev. A **40**, 2410 (1989)
82. Y.M. Ajvasjan, V.V. Ivanov, S.A. Kovalenko, V.M. Baev, E.A. Sviridenkov, H. Atmanspacher, H. Scheingraber: Appl. Phys. B **46**, 175 (1988)
83. V.M. Baev, J. Eschner, J. Sierks, A. Weiler, P.E. Toschek: Opt. Commun. **94**, 436 (1992)
84. V.M. Baev, G. Gaida, H. Schröder, P.E. Toschek: Opt. Commun. **38**, 309 (1981)
85. E.A. Sviridenkov, M.P. Frolov: Kvant. Elektron. **4**, 1028 (1977) [Sov. J. Quantum Electron. **7**, 576 (1977)]
86. V.M. Baev, S.A. Kovalenko, E.A. Sviridenkov, A.F. Suchkov, D.D. Toptygin: Kvant. Elektron. **7**, 1112 (1980) [Sov. J. Quantum Electron. **10**, 638 (1980)]

87. H. Atmanspacher, H. Scheingraber, C.R. Vidal: Phys. Rev. A **32**, 254 (1985)
88. M. Chenevier, M.A. Melieres, F. Stoeckel: Opt. Commun. **45**, 385 (1983)
89. A.A. Kachanov, V.R. Mironenko, K. Pashkovich: Kvant. Elektron. **16**, 146 (1989) [Sov. J. Quantum Electron. **19**, 95 (1989)]
90. A.E. Siegman: Opt. Commun. **5**, 200 (1972)
91. M.B. Klein, C.V. Shank, A. Dienes: Opt. Commun. **3**, 178 (1973)
92. H. Schröder, K. Schultz, P.E. Toschek: Opt. Commun. **60**, 159 (1986)
93. Y. Khanin, A.G. Kagan, V.P. Novikov, M.A. Novikov, I.N. Polushnik, A.I. Shcherbakov: Opt. Commun. **32**, 456 (1980)
94. P. Kumar, G.O. Brink, S. Spence, H.S. Lakkaraju: Opt. Commun. **32**, 129 (1980)
95. A.N. Kolerov: Kvant. Elektron. **15**, 512 (1988) [Sov. J. Quantum Electron. **18**, 325 (1988)]
96. V.V. Vasiliev, V. Egorov, I.A. Chekhonin: Opt. Spektrosk. **58**, 944 (1985) [Opt. Spectrosc. (USSR) **58**, 578 (1985)]
97. Y.H. Meyer, M.N. Nenchev: Opt. Commun. **41**, 292 (1982)
98. V.M. Baev, T.P. Belikova, O.P. Varnavskij, V.F. Gamalij, S.A. Kovalenko, E.A. Sviridenkov: Pis'ma Zh. Eksp. Teor. Fiz. **42**, 416 (1985) [JETP Lett. **42**, 514 (1985)]
99. W.T. Hill III, T.W. Hänsch, A.L. Schawlow: Appl. Opt. **24**, 3718 (1985)
100. V.M. Baev, K.-J. Boller, J. Eschner, A. Weiler, P.E. Toschek: J. Opt. Soc. Am. B **7**, 2181 (1990)
101. F. Stoeckel, G.H. Atkinson: Appl. Opt. **24**, 3591 (1985)
102. K. Thoma, K. Ikushima: J. Radio Res. Lab. **23**, 163 (1976)
103. T. Latz, G. Weirauch, V.M. Baev, P.E. Toschek: Appl. Opt. **38**, 2625 (1999)
104. V.S. Burakov, P.Ya. Misakov, S.N. Raikov: Fresenius' J. Anal. Chem. **355**, 883 (1996)
105. F.G.C. Bijnen, H. Zuckermann, F.J.M. Harren, J. Reuss: Appl. Opt. **37**, 3345 (1998)
106. T.P. Belikova, E.A. Sviridenkov, A.F. Suchkov: Kvant. Elektron. **1**, 830 (1974) [Sov. J. Quantum Electron. **4**, 454 (1974)]
107. T.P. Belikova, E.A. Sviridenkov, A.F. Suchkov: Opt. Spektrosk. **27**, 654 (1974) [Opt. Spectrosc. (USSR) **37**, 372 (1974)]
108. Y. Khanin: *Principles of Laser Dynamics* (Elsevier, Amsterdam 1995)
109. D. Romanini, A. Kachanov, E. Lacot, F. Stoeckel: Phys. Rev. A **54**, 920 (1996)
110. V.M. Baev, V.P. Dubov, E.A. Sviridenkov: Kvant. Elektron. **12**, 2490 (1985) [Sov. J. Quantum Electron. **15**, 1648 (1985)]
111. L.N. Sinitsa: Kvant. Elektron. **4**, 148 (1977) [Sov. J. Quantum Electron. **7**, 77 (1977)]
112. J. Hünkemeier, V.M. Baev, P.E. Toschek: unpublished
113. G. Cerullo, S. De Silvestri, V. Magni: Opt. Lett. **19**, 1040 (1994)
114. L.F. Mollenauer: In *Laser Handbook*, ed. by M.L. Stitch, M. Bass (North-Holland, Amsterdam 1985) pp. 145–230
115. R. Beigang, G. Litfin, H. Welling: Opt. Commun. **22**, 269 (1977)
116. V.P. Kochanov, V.I. Serdyukov, L.N. Sinitsa: Opt. Acta **32**, 1273 (1985)
117. A.D. Bykov, V.A. Kapitanov, O.V. Naumenko, T.M. Petrova, V.I. Serdyukov, L.N. Sinitsa: J. Mol. Spectrosc. **153**, 197 (1992)
118. V.A. Vratskii, A.N. Kolerov: Kvant. Elektron. **12**, 1089 (1985) [Sov. J. Quantum Electron. **15**, 718 (1985)]
119. P.W. France (Ed.): *Optical Fiber Lasers and Amplifiers* (Blackie, Glasgow 1991); J. Schneider, C. Carbonnier, U. Unrau: Appl. Opt. **36**, 8595 (1997)
120. R. Böhm, V.M. Baev, P.E. Toschek: Opt. Commun. **134**, 537 (1997)
121. A.P. Godlevskii, V.P. Lopasov, S.F. Luk'yanenko: Kvant. Elektron. **2**, 701 (1975) [Sov. J. Quantum Electron. **5**, 388 (1975)]
122. W. Brunner, H. Paul: Opt. Commun. **19**, 253 (1976)
123. K.-J. Boller, T. Schröder: J. Opt. Soc. Am. B **10**, 1778 (1993)
124. V.M. Baev, T.P. Belikova, M.P. Ippolitov, E.A. Sviridenkov, A.F. Suchkov: Opt. Spektrosk. **45**, 58 (1978) [Opt. Spectrosc. (USSR) **45**, 31 (1978)]
125. V.E. Zuev, V.P. Lopasov, L.N. Sinitsa: Opt. Spektrosk. **45**, 590 (1978) [Opt. Spectrosc. (USSR) **45**, 331 (1978)]
126. C.E. Moore, M.G.J. Minnaert, J. Houtgast: *The Solar Spectrum from* 2935 Å *to* 8770 Å (Nat. Bur. Stand., Monograph 61, 1966); J.W. Swensson, W.S. Benedict, L. Delbouille, G. Roland: *The Solar Spectrum from* $\lambda = 7498$ Å *to* $\lambda = 12\,016$ Å, *a Table of Measures and Identifications* (Société Royale des Sciences de Liège, Liège 1970)
127. L.S. Rothman, C.P. Rinsland, A. Goldman, S.T. Massie, D.P. Edwards, J.-M. Flaud, A. Perrin, C. Camy-Peyret, V. Dana, J.-Y. Mandin, J. Schroeder, A. McCann, R.R. Gamache, R.B. Wattson, K. Yoshino, K.V. Chance, K.W. Jucks, L.R. Brown, V. Nemtchinov, P. Varanasi: J. Quant. Spectrosc. Radiat. Transfer **60**, 665 (1998)
128. T.J. Latz, G. Weirauch, B. Peters, V.M. Baev, P.E. Toschek: In Proceedings of the International Conference on the Water in the Gas Phase, Paris, June 21–24, 1998, p. 92
129. R.G. Bray, W. Henke, S.K. Liu, K.V. Reddy, M.J. Berry: Chem. Phys. Lett. **47**, 213 (1977)
130. W.T. Hill III, R.A. Abreu, T.W. Hänsch, A.L. Schawlow: Opt. Commun. **32**, 96 (1980)
131. M. A. Mélières, M. Chenevier, F. Stoeckel: J. Quant. Spectrosc. Radiat. Transfer **33**, 337 (1985)
132. A. Campargue, F. Stoeckel, M. Chenevier: Spectrochim. Acta Rev. **13**, 69 (1990)
133. A. Campargue, F. Stoeckel: J. Chem. Phys. **85**, 1220 (1986); D. Permogorov, A. Campargue, M. Chenevier, H. Ben Kraiem: J. Mol. Spectrosc. **170**, 10 (1995)
134. Q.S. Zhu, A. Campargue, F. Stoeckel: Spectrochim. Acta A **50**, 663 (1994)
135. E.N. Antonov, E.B. Berik, V.G. Koloshnikov: J. Quant. Spectrosc. Radiat. Transfer **22**, 45 (1979)
136. Q.S. Zhu, A. Campargue, J. Vetterhöffer, D. Permogorov, F. Stoeckel: J. Chem. Phys. **99**, 2359 (1993)
137. A. Campargue, D. Permogorov: Chem. Phys. Lett. **241**, 339 (1995)
138. O. Vaittinen, L. Biennier, A. Campargue, J.-M. Flaud, L. Halonen: J. Mol. Spectrosc. **184**, 288 (1997)
139. H.H. Hamann, A. Charvat, B. Abel, S.S. Kovalenko, A.A. Kachanov: J. Chem. Phys. **106**, 3103 (1997)
140. M. Hermann, M.I. El Idrissi, A. Pisarchik, A. Campargue, A.-C. Gaillot, L. Biennier, G. Di Lonardo, L. Fusina: J. Chem. Phys. **108**, 1377 (1998)
141. B. Abel, A. Charvat, S.F. Deppe: Chem. Phys. Lett. **277**, 347 (1997)
142. A. Campargue, A. Charvat, D. Permogorov: Chem. Phys. Lett. **223**, 567 (1994)
143. Wm.R. Lambert, P.M. Felker, A.H. Zewail: J. Chem. Phys. **74**, 4732 (1981)
144. N. Goldstein, T.L. Brack, G.H. Atkinson: Chem: Phys. Lett. **116**, 223 (1985); R. Georges, A. Delon, F. Bylicki, R. Jost, A. Campargue, A. Charvat, M. Chenevier, F. Stoeckel: Chem. Phys. **190**, 207 (1995)
145. A. Campargue, D. Permogorov, R. Jost: J. Chem. Phys. **102**, 5910 (1995)
146. N. Goldstein, T.L. Brack, Atkinson: J. Chem. Phys. **85**, 2684 (1986)
147. L.N. Sinitsa: Proc. SPIE **3342**, 93 (1998); L.N. Sinitsa: J. Quant. Spectrosc. Radiat. Transfer **48**, 721 (1992)
148. A. Campargue, F. Stoeckel, M.C. Terrile: Chem. Phys. **110**, 145 (1986)
149. P. Vujkovic Cvijin, W.K. Wells, I. Mendas, J.K. Delaney, J.I. Lunine, D.M. Hunten, G.H. Atkinson: J. Quant. Spectrosc. Radiat. Transfer **49**, 639 (1993)
150. B.B. Radak, J.I. Lunine, D.M. Hunten, G.H. Atkinson: J. Quant. Spectrosc. Radiat. Transfer **52**, 809 (1994); K. Singh, J.J. O'Brien: ibid. **52**, 75 (1994)
151. K. Singh, J.J. O'Brien: J. Quant. Spectrosc. Radiat. Transfer **54**, 607 (1995); K. Singh, J.J. O'Brien: Astrophys. Space Sci. **236**, 97 (1996)
152. B.B. Radak, J.I. Lunine, D.M. Hunten, G.H. Atkinson: J. Quant. Spectrosc. Radiat. Transfer **53**, 519 (1995)
153. G.H. Atkinson: Proc. SPIE **1637**, 126 (1992); J.J. O'Brien, G.H. Atkinson: Chem. Phys. Lett. **130**, 321 (1986)
154. T. Shirafuji, K. Tachibana, Y. Matsui: Jpn. J. Appl. Phys. **34**, 4239 (1995); K. Tachibana, T. Shirafuji, Y. Matsui: ibid. **31**, 2588 (1992)
155. R.A. Akhmedzhanov, I.N. Polushkin, Yu.V. Rostovtsev: Opt. Spektrosk. **76**, 568 (1994) [Opt. Spectrosc. **76**, 505 (1994)]
156. M.J. Lipp, J.J. O'Brien: Chem. Phys. **192**, 355 (1995); A.O. Morozov: Opt. Spektrosk. **81**, 590 (1996) [Opt. Spectrosc. **81**, 538 (1996)]
157. R.J. Thrash, H. von Weyssenhoff, J.S. Shirk: J. Chem. Phys. **55**, 4659 (1971); M. Maeda, F. Ishitsuka, Y. Miyazoe: Opt. Commun. **13**, 314 (1975)
158. M. Maeda, F. Ishitsuka, M. Matsumoto, Y. Miyazoe: Appl. Opt. **16**, 403 (1977)
159. S.J. Harris, A.M. Weiner: Opt. Lett. **6**, 142 (1981)
160. S. Cheskis, S.A. Kovalenko: Appl. Phys. B **59**, 543 (1994)
161. V.S. Burakov, P.A. Naumenkov, S.N. Raikov: Opt. Commun. **80**, 26 (1990)
162. R.A. Keller, E.F. Zalewski, N.C. Peterson: J. Opt. Soc. Am. **62**, 319 (1972); G. Horlick, E.G. Codding: Anal. Chem. **46**, 133 (1974)

163. T.D. Harris, J.W. Mitchell: Anal. Chem. **52**, 1706 (1980)
164. S. Datta, R.W. Anderson, R.N. Zare: J. Chem. Phys. **63**, 5503 (1975)
165. R.V. Ambartsumjan, V.S. Letokhov, S.A. Maksimov, V.I. Mishin, N.P. Furzikov: Kvant. Elektron. **2**, 1851 (1975) [Sov. J. Quantum Electron. **5**, 1018 (1975)]
166. M.V. Belokon, A.N. Rubinov, I.S. Grigor'ev, P.G. Evtukhovich: Zh. Prikl. Spectrosk. **26**, 431 (1977) [J. Appl. Spectrosc. (USSR) **26**, 320 (1977)]
167. G.H. Atkinson, A.H. Laufer, M.J. Kurylo: J. Chem. Phys. **59**, 350 (1973)
168. S.G. Cheskis, O.M. Sarkisov: Chem. Phys. Lett. **62**, 72 (1979)
169. V.P. Bulatov, A.A. Buloyan, S.G. Cheskis, M.Z. Kozliner, O.M. Sarkisov, A.I. Trostin: Chem. Phys. Lett. **74**, 288 (1980)
170. A.A. Ioffe, V.P. Bulatov, V.A. Lozovsky, M.Ya. Goldenberg, O.M. Sarkisov, S.Y. Umansky: Chem. Phys. Lett. **156**, 425 (1989)
171. V.P. Bulatov, A.A. Ioffe, V.A. Lozovsky, O.M. Sarkisov: Chem. Phys. Lett. **159**, 171 (1989)
172. V.P. Bulatov, A.A. Ioffe, V.A. Lozovsky, O.M. Sarkisov: Chem. Phys. Lett. **161**, 141 (1989)
173. O.M. Sarkisov, E.A. Sviridenkov: Zh. Prikl. Spektrosk. **35**, 775 (1981) [J. Appl. Spectrosc. (USSR) **35**, 1184 (1981)]
174. V.M. Baev, O.M. Sarkisov, E.A. Sviridenkov, A.F. Suchkov: J. Sov. Laser Res., Consultants Bureau, New York **10**, 61 (1989)
175. V.A. Lozovsky, O.M. Sarkisov, A.G. Okhrimchuk, A.L. Enis: Chem. Phys. Rep. **16**, 395 (1997)
176. O.M. Sarkisov, V.A. Lozovsky: Proc. SPIE **3342**, 243 (1998)
177. Y.V. Bykov, M.S. Gitlin, M.A. Novikov, I.N. Polushkin, Ya.I. Khanin, A.I. Shcherbakov: Zh. Tekh. Fiz. **54**, 1310 (1984) [Sov. Phys. Tech. Phys. **29**, 755 (1985)]
178. F. Stoeckel, M.D. Schuh, N. Goldstein, G.H. Atkinson: Chem. Phys. **95**, 135 (1985)
179. J.P. Reilly, J.H. Clark, C.B. Moore, G. Pimentel: J. Chem. Phys. **69**, 4381 (1978)
180. N. Goldstein, G.H. Atkinson: Chem. Phys. **105**, 267 (1986)
181. S.G. Cheskis, V.A. Nadtochenko, O.M. Sarkisov: Int. J. Chem. Kinet. **13**, 1041 (1981)
182. V.A. Lozovsky, S. Cheskis, A. Kachanov, F. Stoeckel: J. Chem. Phys. **106**, 8384 (1997)
183. S. Cheskis, I. Derzy, V.A. Lozovsky, A. Kachanov, F. Stoeckel: Chem. Phys. Lett. **277**, 423 (1997)
184. Y.P. Podmar'kov, N.N. Yuryshev, M.P. Frolov: Kvant. Elektron. **22**, 692 (1995) [Quantum Electron. **25**, 665 (1995)]
185. D.J. Eckstrom, J.R. Barker, J.G. Hawley, J.P. Reilly: Appl. Opt. **16**, 2102 (1977)
186. D.C. Miller, J.J. O'Brien, G.H. Atkinson: J. Appl. Phys. **65**, 2645 (1988)
187. Y.M. Efremov, L.V. Gurvich, A.N. Savchenko, E.A. Sviridenkov: Chem. Phys. Lett. **61**, 179 (1979)
188. Y.Y. Kuzyakov, E.N. Moskvitina: Proc. SPIE **3342**, 148 (1998)
189. B. Ståhlberg, V.M. Baev, G. Gaida, H. Schröder, P.E. Toschek: J. Chem. Soc., Faraday Trans. **81**, 207 (1985)
190. V.V. Apollonov, G.G. Baitsur, A.V. Ermachenko, N.A. Raspopov, E.A. Sviridenkov, S.K. Semenov, K.N. Firsov: Kvant. Elektron. **16**, 269 (1989) [Sov. J. Quantum Electron. **19**, 174 (1989)]
191. Y.P. Podmar'kov, M.P. Frolov: Kvant. Elektron. **23**, 611 (1996) [Quantum Electron. **26**, 595 (1996)]
192. N.A. Raspopov, A.N. Savchenko, E.A. Sviridenkov: Kvant. Elektron. **4**, 736 (1977) [Sov. J. Quantum Electron. **7**, 409 (1977)]
193. K. A. Truesdell. R.A. Keller, E.F. Zalewski: J. Chem. Phys. **73**, 1117 (1980)
194. V.M. Baev, K.-J. Boller, A. Weiler, P.E. Toschek: Opt. Commun. **62**, 380 (1987)
195. E. Lacot, F. Stoeckel: In Proceedings of XVI International Conference on Coherent and Nonlinear Optics (Moscow, 29.6–3.7.1998) p. 97
196. V.M. Baev, T.P. Belikova, V.F. Gamalij, E.A. Sviridenkov, A.F. Suchkov: Kvant. Elektron. **11**, 2413 (1984) [Sov. J. Quantum Electron. **14**, 1596 (1984)]
197. V.M. Baev, K.-J. Boller, P.E. Toschek: Opt. Commun. **66**, 225 (1988)
198. W. Werncke, J. Klein, A. Lau, K. Lenz, G. Hunsalz: Opt. Commun. **11**, 159 (1974)
199. V.M. Baev, W. Werncke, E.A. Sviridenkov: Kvant. Elektron. **2**, 856 (1975) [Sov. J. Quantum Electron. **5**, 477 (1975)]
200. A.P. Godlevskii, Y.D. Kopytin: Zh. Prikl. Spectrosk. **29**, 791 (1978) [J. Appl. Spectrosc. **29**, 1301 (1978)]
201. A. Charvát, S.A. Kovalenko, B. Abel: Spectrochim. Acta, Part A **55**, 1553 (1999)
202. A.A. Kachanov, F. Stoeckel, A. Charvat, J.J. O'Brien: Appl. Opt. **36**, 4062 (1997)
203. D. Ong, T. Latz, V.M. Baev, P.E. Toschek: unpublished
204. A.L. Schawlow, C.H. Townes: Phys. Rev. **112**, 1940 (1958)
205. N. Dutta, R.T. Warner, G.J. Wolga: Opt. Lett. **1**, 155 (1977)
206. E. Kleist, H. Bettermann: Opt. Lett. **13**, 449 (1988)
207. W. Gurlit, J.P. Burrows, H. Burkhard, R. Böhm, V.M. Baev, P.E. Toschek: Infrared Phys. Technol. **37**, 95 (1996)
208. H. Bettermann: Spectrochim. Acta, Part A **50**, 1073 (1994)
209. H.K. Holt: Phys. Rev. A **11**, 625 (1974); **14**, 1901 (1976)
210. H.J. Kimble: IEEE J. Quantum Electron. **QE-16**, 455 (1980)
211. N. Djeu: J. Chem. Phys. **60**, 4109 (1974)
212. E. Lacot, F. Stoeckel, D. Romanini, A. Kachanov: Phys. Rev. A **57**, 4019 (1998)
213. S.A. Batishche, V.A. Mostovnikov, A.N. Rubinov: Kvant. Elektron. **3**, 2516 (1976) [Sov. J. Quantum Electron. **6**, 1386 (1976)]
214. F. Träger, R. Neumann, J. Kowalski, G. zu Putlitz: Appl. Phys. **12**, 19 (1977)
215. M. Barnes, D.J. Clouthier, P.G. Hajigeorgiou, G. Huang, C.T. Kingston, A.J. Merer, G.F. Metha, J.R.D. Peers, S.J. Rixon: J. Mol. Spectrosc. **186**, 374 (1997)
216. C. Zhu, H.G. Kjaergaard, B.R. Henry: J. Chem. Phys. **107**, 691 (1997)